ANALYSIS OF NOSETIP BOUNDARY LAYER TRANSITION MECHANISMS

Charles L. Merkle, et al

Flow Research, Incorporated

Prepared for:

Air Force Office of Scientific Research

July 1975

FLOW RESEARCH, INC.

AIR FORCE OFFICE OF SCIENTIFIC RESEARCH (AFSC)
NOTICE OF TRANSMITTAL TO DDC
This technical report has been reviewed and is approved for public release IAW AFR 190-12 (7b).
Distribution is unlimited.
A. D. BLOSE
Technical Information Officer

Approved for public release; distribution unlimited.

FLOW RESEARCH, INC.

- 1819 S. Central Avenue, Kent, Wash. 98031, (206) 854-1370, 854-9590
- 5959 W. Century Blvd., Los Angeles, Calif. 90045, (213) 641-4931
- 1 Broadway, Cambridge, Mass. 02142, (617) 876-3400

UNCLASSIFIED

SECURITY CLASSIFICATION OF THIS PAGE (When Data Entered)

REPORT DOCUMENTATION PAGE		READ INSTRUCTIONS BEFORE COMPLETING FORM
1. REPORT NUMBER AFOSR - TR - 75 - 1462	2. GOVT ACCESSION NO.	3. RECIPIENT'S CATALOG NUMBER
4. TITLE (and Subtitle) ANALYSIS OF NOSETIP BOUNDARY LAYER TRANSITION MECHANISMS		5. TYPE OF REPORT & PERIOD COVERED INTERIM 16 July 1974-15 July 1975 6. PERFORMING ORG. REPORT NUMBER Report No 60
7. AUTHOR(s) DENNY R S KO TOSHI KUBOTA CHARLES L MERKLE WALTER J GRABOWSKI		8. CONTRACT OR GRANT NUMBER(s) F44620-74-C-0049
9. PERFORMING ORGANIZATION NAME AND ADDRESS FLOW RESEARCH, INC 9841 AIRPORT BOULEVARD, SUITE 1004 LOS ANGELES CAIFORNIA 90045		10. PROGRAM ELEMENT, PROJECT, TASK AREA & WORK UNIT NUMBERS 681307 9781-02 61102F
11. CONTROLLING OFFICE NAME AND ADDRESS AIR FORCE OFFICE OF SCIENTIFIC RESEARCH/NA 1400 WILSON BOULEVARD ARLINGTON, VIRGINIA 22209		12. REPORT DATE July 1975 13. NUMBER OF PAGES 75
14. MONITORING AGENCY NAME & ADDRESS(if different from Controlling Office)		15. SECURITY CLASS. (of this report) UNCLASSIFIED 15a. DECLASSIFICATION DOWNGRADING SCHEDULE

16. DISTRIBUTION STATEMENT (of this Report)

Approved for public release; distribution unlimited.

17. DISTRIBUTION STATEMENT (of the abstract entered in Block 20, if different from Report)

18. SUPPLEMENTARY NOTES

19. KEY WORDS (Continue on reverse side if necessary and identify by block number)

BOUNDARY LAYER
TRANSITION
STABILITY THEORY
TURBULENCE
REENTRY

20. AUSTRACT (Continue on reverse side if necessary and identify by block number)

Linear stability theory is being used to investigate the mechanisms which lead to boundary layer transition on re-entry vehicle nosetips. Specific efforts are aimed at determining the effects of various parameters including surface roughness, ablation, wall cooling, local Mach numbers, pressure gradient, and axisymmetric geometry on transition. Roughess is simulated by means of the "turbulent sublayer" model which has been extended to compressible flow. Results indicate that both roughness and ablation strongly reduce the transition Reynolds number. A series of parametric stability solutions has been calculated for

DD FORM 1 JAN 73 1473 EDITION OF 1 NOV 65 IS OBSOLETE

UNCLASSIFIED

SECURITY CLASSIFICATION OF THIS PAGE (When Data Entered)

non-zero pressure gradient cases. Results show that even at the subsonic Mach numbers which characterize nose-tip boundary layers, the effects of compressibility have substantially altered the stability characteristics of the boundary layer. Computations of the stability characteristics of an actual nosetip boundary layer indicate that for smooth-wall cases, all types of disturbances are stable and that the margin of stability is considerable. Inclusion of realistic roughnesses rapidly lowers the critical Reynolds number. Thus far, rough-wall solutions have been completed only near the stagnation point where the boundary layer is till stable to all disturbances. Additional computations further around the nosetip are in progress.

FLOW RESEARCH REPORT NO. 60

ANALYSIS OF NOSETIP BOUNDARY LAYER TRANSITION MECHANISMS*

FINAL REPORT

By

Charles L. Merkle

Walter J. Grabowski

Toshi Kubota

Denny R.S. Ko

JULY, 1975

Flow Research, Inc.
1819 South Central Avenue
Kent, Washington 98031
(206) 854-1370

*This work supported by AFOSR Contract No. F44620-74-C-0049.

ANALYSIS OF NOSETIP BOUNDARY LAYER TRANSITION MECHANISMS*

by

Charles L. Markle
Walter J. Grabowski
Toshi Kubota
Denny R.S. Ko

ABSTRACT

Linear stability theory is being used to investigate the mechanisms which lead to boundary layer transition on re-entry vehicle nosetips. Specific efforts are aimed at determining the effects of various parameters including surface roughness, ablation, wall cooling, local Mach numbers, pressure gradient, and axisymmetric geometry on transition. Roughness is simulated by means of the "turbulent sublayer" model which has been extended to compressible flow. Results indicate that both roughness and ablation strongly reduce the transition Reynolds number. A series of parametric stability solutions has been calculated for non-zero pressure gradient cases. Results show that even at the subsonic Mach numbers which characterize nosetip boundary layers, the effects of compressibility have substantially altered the stability characteristics of the boundary layer. Computations of the stability characteristics of an actual nosetip boundary layer indicate that for smooth-wall cases, all types of disturbances are stable and that the margin of stability is considerable. Inclusion of realistic roughnesses rapidly lowers the critical Reynolds number. Thus far, rough-wall solutions have been completed only near the stagnation point where the boundary layer is still stable to all disturbances. Additional computations further around the nosetip are in progress.

*This work supported by AFOSR Contract No. F44620-74-C-0049.

TABLE OF CONTENTS

LIST OF FIGURES

NOMENCLATURE

A	Local amplitude of disturbance in boundary layer.
A_o	Initial amplitude of boundary-layer disturbances.
A^+	Constant in wall roughness model, see Eq. (18).
B'	Dimensionless blowing rate, $B' = (\rho_w v_w/\rho_e u_e)St$.
C	Density-viscosity product, see Eq. (17).
c_p	Specific heat at constant pressure.
F	Velocity variable in transformed momentum equation; $F' = u/u_e$. Also, non-dimensional frequency, $F = \omega\nu/u_e^2$.
$\tilde{F}$	Non-dimensional frequency in rotated coordinate system; $\tilde{F} = F/\cos^2\psi$.
G	Non-dimensional enthalpy in transformed energy equation; $G = H/H_e$.
H	Stagnation or total enthalpy; also, shape factor, $H = \delta^*/\theta$.
K_c	Constant in wall roughness model, see Eq. (18).
k	Molecular thermal conductivity; also used to signify roughness height.
k_T	"Total" thermal conductivity; sum of molecular plus "turbulent" conductivity in near wall region.
M	Mach number.
p	Pressure.
Pr	Prandtl number, $\mu C_p/k$.
Pr_T	"Total" or effective Prandtl number, see Eq. (9).
R	Square root of Reynolds number, $R = \sqrt{Re_x}$.
$\tilde{R}$	Reynolds number in rotated coordinate system, $\tilde{R} = R\cos\psi$.
r_o	Locus radius of axisymmetric body.
Re	Reynolds number.
Re_k	Roughness Reynolds number, $Re_k = u_k k/\nu_k$.

NOMENCLATURE (cont'd)

S	Arc-length distance along surface measured from stagnation point.
St	Stanton number.
T	Temperature.
t	Time.
u,v	Velocity components in cartesian (or axisymmetric) coordinate system.
u_k	Velocity at top of roughness element.
x,y	Cartesian coordinate system; x is streamwise direction; y may also refer to radial coordinate axisymmetric system.
α	Complex wave number of fluctuating quantity.
β	Falkner-Skan pressure gradient parameter. $\beta = \frac{2\xi}{M_e}\frac{dM_e}{d\xi}$ in Levy-Lees coordinates.
β_1	Constant in wall roughness model, see Eq. (18).
γ	Ratio of specific heats.
δ	Boundary-Layer thickness.
δ_k	Representative boundary-layer thickness.
δ^*	Boundary-Layer displacement thickness.
ϵ	Eddy viscosity for momentum transport.
ϵ_H	Eddy conductivity for transport of heat.
η	Transformed normal (to the wall) coordinate in Levy-Lees system; see Eq. (12).
θ	Momentum thickness of boundary layer.
μ	Molecular viscosity.
μ_T	"Total" viscosity, sum of molecular plus "turbulent" viscosities in near-wall region.
ν	Kinematic viscosity, $\nu = \mu/\rho$.
ξ	Transformed streamwise coordinate in Levy-Lees system; see Eq. (11).

NOMENCLATURE (cont'd)

ρ	Density.
τ_w	Skin friction at the wall.
ϕ	Refers to a general variable; azimuthal coordinate in cylindrical coordinate system.
ψ	Angle of skewness of three-dimensional wave. $\psi = 0$ corresponds to wave whose direction of propagation is in the x-direction.
ω	Frequency of fluctuating quantity.

Superscripts

$\overline{}$	Signifies time-averaged part of unsteady quantity.
$'$	Signifies fluctuating part of unsteady quantity; also indicates differentiation.
$\hat{}$	Signifies amplitude of a fluctuating quantity.
ω	Exponent relating viscosity to temperature.

Subscripts

CR	Critical condition.
e	Conditions evaluated at the edge of the boundary layer.
i	Imaginary part of a complex number.
k	Conditions evaluated at the top of roughness elements; or referring to roughness.
w	Conditions evaluated at the wall.
∞	Conditions evaluated far upstream from the body.

1. INTRODUCTION

As a vehicle re-enters the atmosphere, its entire surface is initially embedded within an all-laminar boundary layer, and transition to turbulence occurs in the wake behind the body. During the descent, the location of transition moves progressively closer to the body, reaches the rear skirt of the vehicle, and continues to move toward the nose of the vehicle in a more or less steady fashion. During this time, certain anomalies in the flight path, or in atmospheric conditions, may cause the transition location to remain stationary for a time, or even to move backwards momentarily; however, after some critical condition has been surpassed, the transition location ceases this gradual forward motion and instantaneously jumps from the conical section of the vehicle onto the nosetip. Experiments and flight data alike have shown that the nosetip location is a stable location and that transition is not likely to jump again to the aft-end of the vehicle. After the transition point has jumped to the nosetip, it once again resumes its forward progression, moving toward the nosetip stagnation point.

When the transition region is on the nosetip, a potentially strong interaction exists between the high local heat transfer rates which occur in the vicinity of the transition region and the regression rate of the ablative nosetip surface. Of course, the surface of the entire nosetip regresses as the body descends, but the high transitional heating causes increased local ablation rates which can lead to radical changes in the shape of the nosetip, especially if the transition location remains at a fixed position on the nosetip for a time. A more complete understanding of the mechanisms which cause transition to occur on the nosetip would enable the designer to minimize the thickness of the ablative shield which is used on the nosetip, while still maintaining an adequate margin of safety, and to predict more accurately the ballistic trajectory of the re-entering vehicle. Such knowledge could also be used to select the flight path in a manner which would minimize the tendency to create radical shape deformations.

The mechanisms which control the position of the transition region when it occurs on the nosetip are many. Among them are the free-stream Mach number, the local Mach number distribution at the edge of the boundary layer, the Reynolds number, the wall temperature, the surface roughness and the surface ablation rate. Of these various parameters, the block of experimental transition data which has been amassed in the past few years under the PANT Program (Powars, 1973; Anderson,

1974) suggests that the roughness characteristics of the nosetip surface most strongly influence the location of transition. A second significant parameter is the wall-to-free-stream enthalpy ratio which can have particularly important effects in the presence of wall roughness. Although these experimental results have greatly increased our knowledge of the transition behavior on the nosetip, significant gaps still exist in our understanding. Effects of changes in body geometry (either design changes or changes caused by ablation) are poorly understood, as are effects of scaling the body size. This report summarizes the current results and status of an on-going analytical research program which is aimed at obtaining improved understanding of the mechanisms which lead to transition on the nosetip, and at identifying the effect of, and the relative importance of, the various parameters which affect transition. Although the effects of roughness and ablation are dealt with in the present report, only their direct effect on transition is considered; no description of the coupling between the boundary layer and the shape of the surface, or its roughness characteristics, is included. Finally, it is noted that even though nosetips with rough surfaces and finite rates of heat transfer are of primary interest, the study of smooth-walled nosetips and adiabatic nosetips can also be helpful in elucidating transition mechanisms. Some discussion of these effects is presented later.

2. TRANSITION MECHANISMS AND THEIR THEORETICAL DESCRIPTION

Before discussing methods for describing the transition phenomena, it is desirable to outline, in as much detail as possible, the events which occur during boundary layer transition. The most careful and thorough experiments which have been conducted to examine transition from a "microscopic" viewpoint are the series of experiments which have been carried out at the National Bureau of Standards (Schubauer and Skramstad, 1948; Schubauer and Klebanoff, 1956; Klebanoff, Tidstrom, and Sargent, 1962). Although these measurements were taken in incompressible, flat plate boundary layers, we anticipate that many of the same phenomena which were observed in these experiments will also take place in a typical nosetip boundary layer. To be sure, certain differences may also be expected; these are mentioned later.

2.1 Experimental Observations

If we observe the development of a boundary layer from the leading edge of a flat plate to a distance which is sufficiently far downstream that the boundary layer has become fully turbulent, we can distinguish a number of distinct regions. In the first region, the boundary layer is laminar, and if small disturbances are introduced into the boundary layer, they will decay in amplitude as they are swept downstream. After the boundary layer has reached a particular thickness (*i.e.*, when the local Reynolds number becomes large enough), disturbances within a particular narrow frequency band will be amplified as they are swept downstream, while others will continue to be damped. Comparisons with boundary layer stability theory indicate that those waves which grow (as well as those which decay) are closely described by the linear theory. Consequently, this region can be referred to as a region of linear growth.

Following the region of linear growth is a region of non-linear growth. The precise location at which the non-linear effects become important depends upon the amplitude of the disturbances inside the boundary layer. This has been demonstrated experimentally by Klebanoff *et al.* (1962) by introducing artificial disturbances into the boundary layer upstream of the non-linear growth region and observing their effect on the transition location. As the amplitude of these external disturbances was increased, the length of the linear region decreased, non-linear effects began sooner, and the transition location moved toward the leading edge of the plate. For sufficiently large external disturbances, the linear growth region was completely eliminated. The manner in which the non-linearities enter is particularly significant. They first appear as a modification of the mean flow profiles; the build-up of harmonic frequencies in this initial non-linear region is observed to be small. The physical meaning of this interaction between the unsteady disturbances and the mean flow is obvious: energy is extracted from the mean flow to feed the growing disturbances. In the simplest theoretical description, this interaction is described by the non-zero correlation between the streamwise and the vertical velocity fluctuations, $\langle u'v' \rangle$.

One remaining aspect of the non-linear growth region in flat plate, transitional, boundary layers is of particular interest. First of all, these non-linear effects, even in a two-dimensional boundary layer, have a pronounced three-dimensional nature. The interaction between the waves and the mean flow result in periodic spanwise variations in the mean flow profiles. (The

axisymmetric realization of these planar three-dimensional effects would appear to be a significant unknown quantity in the nosetip problem.) At some spanwise locations, the profile has become slightly fuller than the Blasius profile, while at intermediate locations, a distinct point of inflection has been developed. It is in this inflectional profile that the onset of the next region is noted, namely, the intermittent appearance of turbulent spots. These turbulent spots are generated in the inflectional portions of the boundary layer profile because of a secondary instability which exhibits a very rapid, almost explosive, amplification which causes the high frequency content of the disturbances to increase rapidly, resulting in the birth of a turbulent spot. It is interesting to note that this streamwise location (where turbulent spots begin) is one of the earliest locations which is used in experimental investigations as a measure of the "beginning" of transition. However, as noted, a variety of fundamentally important transition phenomena have already taken place before the turbulent spot appears.

Following the appearance of turbulent spots, comes the final region in which turbulence spreads to encompass the entire boundary layer leading to the familiar fully turbulent characteristics. In this region the mean velocity profiles develop their very full turbulent shape, and the skin friction and heat transfer coefficients at the wall increase to their fully turbulent values.

In summary, a number of observations can be made. First of all, it is clear that significant "transitional" events occur before the "beginning" of transition as measured in typical experiments. Any method which is aimed at determining the mechanisms which lead to transition must include these phenomena. Second, the initial mean velocity profile deformations which occur in the boundary layer are three-dimensional in nature, but it is the inflectional profiles which act to generate turbulence. As the profile deforms from its original Blasius shape to its final turbulent shape, it first deforms to an inflectional profile (*i.e.*, a less full profile) and then reverts to the full turbulent profile. Thus, the deformation of the velocity profile is not a monotonic deformation from the Blasius shape to the turbulent profile. A third observation is that the initial linear amplification region frequently consumes the largest percentage of the distance to the initial turbulence breakdown location. In other words, the nonlinear amplification mechanisms are quite strong and take place very rapidly (over a short distance); implicit use of this observation has been made in our linear-stability based analysis which is described below. Finally, it is noted

that the waves which are observed to grow in the pre-transitional boundary layer are much lower in frequency than are typical turbulence phenomena. The higher frequencies which are characteristic of turbulence do not appear until the secondary instability has begun.

All the above discussion pertains to transition on a flat plate, and although we can expect to see some similarities between the flat plate and the nosetip boundary layers, we also anticipate that there will be some differences. The most striking difference is the pressure gradient in the two problems. Whereas the above-described flat plate data was obtained under constant free-stream velocity and zero pressure gradient conditions, the nosetip flow field is characterized by the strongly favorable pressure gradient conditions which are representative of the expansive flow away from an axisymmetric stagnation point. (If the pressure gradient on the nosetip is expressed in terms of the familiar Falkner-Skan parameter, β, the nosetip has a value of $\beta = 0.5$, while the flat plate has a value of $\beta = 0$.) One might expect the mechanisms which control transition in this highly favorable pressure gradient to be somewhat different than those which are observed on a flat plate. Our analysis bears this out. Similar differences might be expected due to the axisymmetric geometry, the compressibility effects and the wall cooling effects which occur on the nosetip. Ablation and wall roughness are also expected to influence the transition mechanisms on a nosetip as indicated above.

2.2 Methods for Predicting Transition Locations

A number of methods for predicting the location of transition have been proposed. These methods range from purely empirical ones to methods which solve the complete unsteady Navier-Stokes equations. Empirical methods are generally concerned with correlating the macroscopic results of transition testing; that is to say, empirical methods try to predict the magnitude and the direction of the change in the transition Reynolds number which is caused by a corresponding change in some parameter (such as the Mach number, the free-stream unit Reynolds number, *etc.*). Quite naturally, most correlation techniques are based partially on theoretical principles (and as such should be classified semi-empirical theories).

Some of the more recent correlation techniques which are used for the nosetip transition problem are the one which has been developed by Anderson (1973) and the one being developed by White (1974). These techniques, which

combine current theoretical understanding of the nosetip problem with the available experimental data, have resulted in useful engineering correlations for a limited range of parameters.

The extension of phenomenological turbulence-modelling theories to low Reynolds number ranges in the hope of describing the characteristics of the transitional boundary layer has also become increasingly popular. This approach was originally proposed by Donaldson (1969), and applications of his basic approach to the nosetip problem are currently being attempted by Finson *et al.* (1974) and Wilcox (1974). The turbulence modelling approach, when combined with a finite-difference solution of the equations of motion, has the attractive appeal that it gives "exact" results in the laminar region of the boundary layer, and contains a phenomenological turbulence model which has been adjusted to give reasonable results in the turbulent flow regime. Thus, the only portion of the boundary layer which is missing is the transitional part. Several turbulence codes (*e.g.*, Mellor and Herring, 1972; Beckwith and Bushnell, 1967) include this region by a "switch" which gradually "turns on" the turbulence model during the transitional region. The location of transition is specified by means of a semi-empirical correlation. No attempt is made to include any of the physics of transition in the computation of the transitional region. The approaches of Donaldson, Finson *et al.*, and Wilcox represents attempts to extend the applicability of the turbulence models to low Reynolds numbers by including some of the physics of transition in the model. These approaches, then, basically become experimental data correlation techniques which use partial differential equations rather than algebraic equations. Whether or not any attempt is made to model some of the physics in the transitional boundary layer, turbulence-model approaches have the advantage (and the disadvantage!) that they always yield a solution to the complete laminar-transitional-turbulent boundary layer. Further, if sufficient data exists to define the arbitrary constants and functions in the models, these turbulence approaches can be effectively used to interpolate between existing sets of experimental results. Since they contain only a minimal amount of physics (particularly as regards the early portions of transition where the turbulence which they model does not yet exist), the turbulence model approaches cannot be reliably extrapolated to flow regimes for which they have not been adjusted, nor can they be used to study the mechanisms of transition. Like the other data-correlation methods, they can only attempt to predict macroscopic

effects in the transitional boundary layer. A further discussion of the use of turbulence models for transition calculations and comparison with the linear stability technique is given in Section 5.

The most ambitious approach to predicting boundary-layer transition is through the numerical solution of the full, unsteady Navier-Stokes equations. It is normally assumed that the solutions of the unsteady Navier-Stokes equations contain the complete phenomena of transition; however, as indicated above, the full three-dimensional equations must be used to obtain realistic results. This requires enormous amounts of computational storage and time, and problems of sub-grid scale fluctuations must still be overcome. Despite the difficulties, progress in this direction has been reported by Orszag (1974) and Grosch (1974), but at the present time this technique remains too expensive for use in predicting the flows over realistic bodies.

2.3 The Use of Linear Stability Theory for Investigating the Mechanisms of Transition

The method we have used for our analysis of the mechanisms which lead to transition is based on linear stability theory. Like the numerical solution of the complete Navier-Stokes equations, the linear stability approach represents an exact solution of the unsteady Navier-Stokes equations in the early portions of the pre-transitional boundary layer. However, like the semi-empirical correlation techniques and the turbulence models, the linear stability approach cannot predict transition locations without some empirical input. The reason for this is simply that transition is an inherently non-linear phenomena. For example, transition cannot occur until non-linear interactions between the wave-like disturbances and the mean flow profiles have taken place. Nevertheless, as indicated above, much of the controlling growth of disturbances inside the boundary layer can be accurately described by the linear theory in many instances, and this represents virtually the only promising theoretical approach to take if an understanding of the transition mechanism is desired.

The equations of linear stability theory are obtained from the unsteady, Navier-Stokes equations by expressing each of the dependent variables in terms of a steady mean-flow component and an unsteady fluctuating component. Thus, for a general property ϕ, we have

$$\phi = \bar{\phi}(x,y) + \phi'(x,y,z,t) \ , \qquad (1)$$

for a two-dimensional boundary layer. When expressions of this form are substituted into the equations of motion, the barred quantities lead to the standard boundary layer equations (after an appropriate ordering of terms has been made), whereas the primed terms lead to the stability equations. A complete derivation of these equations is given in standard textbooks for the incompressible case; the most complete drrivation for the compressible case is given by Mack (1969).

The stability equations are traditionally solved by Laplace transform techniques in time, and Fourier transform techniques in the streamwise direction. For example, the perturbation, ϕ', can be expressed as

$$\phi'(x,y,t) = \phi(y) \exp\left[i(\alpha x - \omega t)\right] . \qquad (2)$$

Upon substitution of expressions of this form into the linear stability equations, we obtain a set of coupled, ordinary differential equations in the cross-stream variable, y. The resulting set of ordinary differential equations can then be solved by standard numerical techniques. Since these ordinary differential equations are homogeneous, and since the corresponding boundary conditions are likewise homogeneous (*see* Mack, 1969, for details), the only solution which can be obtained (other than a trivial solution) is an eigenvalue solution. If the frequency, ω, is taken as purely real, while the wave number, α, is allowed to be complex, the spatial amplification rate of a wave of a particular frequency and Reynolds number can be obtained as the eigenvalue of the system. If the amplification rate of a single frequency disturbance is computed at each of a number of streamwise locations in the boundary layer (with the boundary layer being assumed to be locally parallel, but of a different thickness at each location), the resulting amplitude of this wave, in terms of its amplitude at some reference location, is

$$A(\omega)/A_o(\omega) = \exp\left[-\int \alpha_i(x,\omega)dx\right] , \qquad (3)$$

where a dependence on the frequency is assumed.

The adaptation of linear stability theory to the problem of predicting the significance of various parameters on transition is achieved by tabulating the dependence of the amplification rate, $-\alpha_i$, on these parameters (by solutions of the linear stability equations). It should be noted that, at this stage, the analysis is still completely analytical; no empirical information has been included. The response of disturbances of various frequencies, and

their net growth or decay can be obtained directly from the equations of motion. This represents one of the most attractive features of the linear stability approach to transition; it includes the physics of the pre-transitional boundary layer (so long as disturbances are small), and it is simple enough to be tractable. Methods for applying these stability results to the actual prediction of transition are given below.

2.4 Transition Criteria for Use with Linear Stability Theory

In order to link the linear stability theory with transition, some empirical transition criterion is necessary. If the non-linear effects were included in the stability calculations, such an empirical criterion could, in principle, be bypassed, although it would probably still be practical to include it. One of the most widely used techniques for predicting boundary layer transition is the e^9 method suggested by Smith and Gamberoni (1956), and used in our previous work, Merkle, Kubota and Ko (1974). In the e^9 method, the growth of disturbances is computed by linear stability theory until an empirically defined level of amplification has been exceeded, at which time, transition is said to occur. Although an amplification of e^9 is reasonable in incompressible flows, it is considerably too large for compressible boundary layers, where transition can frequently occur when the disturbances, as predicted by linear stability theory, have grown by only a factor of e^2 (Merkle, Kubota and Ko, 1974). A potentially useful empirical transition criterion for compressible boundary layers was suggested by Mack (1975). In this approach, the initial disturbance levels in the boundary layer are related to the free stream disturbances by means of an empirical formula. Then the growth of disturbances is computed by linear stability theory, with transition being predicted when the amplitude of the disturbance reaches a particular level. With this approach, Mack was able to use a single transition criterion for all supersonic boundary layers, but he still was forced to use a different relation for subsonic boundary layers. We have not as yet used this criterion in our nosetip transition predictions, but plan to test it in the future.

3. PREDICTION OF THE EFFECTS OF VARIOUS PARAMETERS ON TRANSITION

This section presents some transition predictions which have been obtained by applying the results of linear stability theory. In order to assess their accuracy, these predictions are compared with appropriate wind-tunnel measurements. The general objective of these comparisons is to evaluate the capability of the stability approach to predict the effects of various parameters on the location of transition.

3.1 The Effect of Reynolds Number-per-Inch

Measurements of the location of transition on a model in a supersonic wind-tunnel have consistently shown that transition depends on the Reynolds number-per-inch of the free-stream flow. Similarly, transition measurements of the same model in different wind-tunnels has shown substantial variations. These variations in the transition location have been frequently attributed to tunnel-to-tunnel differences in the free-stream disturbance levels, or on variations in the disturbance levels within a single tunnel with Reynolds number-per-inch. In fact, Pate and Schueler (1969) and Pate (1971) correlated a wide range of data solely on the basis of the acoustic environment in the wind-tunnel. Their results suggest that the transition location on a flat plate or a cone is independent of Mach number, and depends only on the disturbance environment.

In order to predict the observed Reynolds number-per-inch variations in the location of transition, the linear stability results must be coupled with a transition criterion which depends upon the initial disturbance level in the boundary layer.

The e^n transition criterion which has been developed by Smith and Gamberoni (1956) indicates that transition will occur when disturbances within the boundary layer have grown by a specific (empirically determined) factor. However, this link between the total amplification of disturbances and transition is based upon an implicit assumption that the initial disturbance levels are similar from case to case. In situations in which the initial disturbance level changes, the e^n criterion (which is based on total amplification) should be replaced by an amplitude criterion which assumes that transition will begin when the disturbance level inside the boundary layer reaches a particular threshold value. The use of such an amplitude criterion, which explicitly accounts for the initial disturbance level, would lead to earlier transition predictions in "noisy" wind tunnels than in "quiet" wind tunnels. By inference,

the corresponding amplification ratios, A/A_o, at the predicted transition location will be smaller for the noisy wind-tunnel case than for the quiet wind-tunnel case. We believe that this interpretation of the e^n method is in the same spirit that Smith originally intended the method to be used.

Before discussing the transition predictions, it is worthwhile to review the general character of wind-tunnel disturbances.

It is well-known that small disturbances in compressible flows can be grouped into one of three types, namely, vorticity fluctuations, pressure fluctuations, and entropy fluctuations. Of these three types of disturbances, the vorticity fluctuations in the wind-tunnel free-stream flow dominate the effect of free-stream disturbances on transition at low Mach numbers, whereas the pressure, or acoustic, fluctuations dominate the transition behavior at higher (above Mach 2.0) wind-tunnel speeds. It appears that entropy fluctuations are of minor importance except perhaps in the case of heated-inlet wind-tunnel testing.

Experimental results of the effect of free-stream turbulence on transition Reynolds numbers were reported by Schubauer and Klebanoff (1952) and a composite curve was given by Dryden (1954). The combined effects of turbulence and acoustic waves on the location of transition has been measured by Spangler and Wells (1969). The results of these experiments are summarized in Fig. 1, and show that transition can behave very differently under the influence of different types of free-stream disturbances.

Nosetip transition tests are generally run at high supersonic wind-tunnel Mach numbers where the effects of acoustic disturbances are generally more significant than are the effects of free-stream turbulence. Laufer (1964) has shown that the acoustic energy in the free-stream is approximately proportional to the free-stream dynamic pressure. This acoustic energy, which is radiated by the boundary layers on the wind-tunnel walls, also scales directly with the skin friction. Thus, as the Reynolds number-per-inch of the flow is increased, the Reynolds number of the wall boundary layer increases and (assuming the Reynolds number is sufficiently high that the wall boundary layer is turbulent), the skin friction coefficient decreases. As a result, the acoustical disturbance level in the boundary layer decreases as the Re/in. is increased. This suggests that the transition Reynolds number would increase with the tunnel Re/in. (Specifically, if transition occurs when the disturbance amplitude reaches a critical level, and if the initial level is lowered, then

more amplification is required and transition moves to higher Reynolds numbers.) The experimental results show that this is the proper qualitative trend.

An experimental measure of the changes in the transition Reynolds number with Reynolds number-per-inch is shown in Fig. 2. In these experiments, which were performed by Pate and Schueler (1969), the free-stream acoustic disturbance level was measured, and we have used the acoustic disturbance level as the abscissa in Fig. 2. As can be seen, the experimental results indicate lower transition Reynolds numbers as the acoustic disturbance increases in energy. The corresponding transition predictions, which have been based on the results of stability theory, and a maximum amplitude transition criterion, are also shown in the figure. (For these results, the maximum amplitude criterion was selected to give the proper transition Reynolds number at one point. Thus, the level of the predictions has been adjusted to fit the data; only the rate of change of the predictions with the acoustic environment is meaningful.) For both the $M_\infty = 3.0$ and $M_\infty = 5.0$ cases, the predictions indicate the correct qualitative trends, but underpredict the effect. This discrepancy could be attributed to a number of factors. For example, the reported transition locations are end-of-transition locations. Stability theory should not be used for end-of-transition predictions; only for beginning-of-transition predictions. Nevertheless, we believe that the underprediction of the effect of free-stream disturbances is more fundamental than this. Stability theory indicates that transition is very dependent on the frequency of the external disturbance environment as well as its level. An estimate of the frequency spectrum of the disturbances (which is not recorded) should be included in the initial disturbance levels, A_o. Such an estimate could be obtained from the spectral measurements of Laufer (1964). However, Mack (1974), using other data sources, has reported that the inclusion of the frequency dependence is still not enough to predict the observed variations in Re/in. In his latest work, Mack (1975) has shown that the disturbance level and its frequency distribution must be combined with a strongly non-linear relationship between free-stream disturbances and boundary-layer disturbances in order to successfully predict the observed Re/in. effects. This relationship represents the receptivity of the boundary layer to disturbances from the free-stream, and suggests that they can be damped or amplified as they interact with the boundary layer. Similar conclusions can be reached by solving the "forced" problem of stability theory (Mack, 1971).

3.2 Extension of Turbulent Sublayer Model to Compressible Flow

In a previous report (Merkle, Kubota, and Ko, 1974), we developed a "turbulent sublayer" model to describe the effects of distributed surface roughness on transition. This turbulent sublayer model is based on the experimental observations of Klebanoff and Tidstrom (1972) which indicated that surface roughness affects transition in two distinct manners; (1) roughness modifies the mean velocity profiles, and (2) roughness increases the initial disturbance level inside the boundary layer. The observed modifications in the mean flow profiles decreased the critical Reynolds number below its smooth-wall value, and increased the rate of amplification of disturbances in the (enlarged) unstable region. When coupled with the higher initial disturbance levels, this increased amplification rate led to substantial reductions in the transition Reynolds number.

The turbulent sublayer model visualizes the distortions in the mean flow profiles as being the result of an enhanced momentum transfer near the wall which is caused by an unsteadiness in the viscous flow over the individual roughness elements. The quantitative effects of this enhanced momentum transfer are included in the computation of the mean flow profiles by means of an eddy viscosity formulation.

In our previous report, this model was used to predict the location of transition for a series of incompressible boundary layers, including both favorable and unfavorable pressure gradient cases. Before being applied to nosetip boundary layers, the turbulent sublayer model must be extended to compressible flow. This extension has been accomplished by introducing an eddy diffusivity to represent the enhanced heat transfer in the region near the rough surface. This eddy diffusivity was then defined in terms of the momentum eddy viscosity and a turbulent Prandtl number (which was taken as unity). An outline of this development follows.

The equations for a compressible, laminar boundary layer are (Hayes and Probstein, 1959),

$$\frac{\partial}{\partial x}\rho u r_o + \frac{\partial}{\partial y}\rho v r_o = 0 \tag{4}$$

$$\rho u \frac{\partial u}{\partial x} + \rho v \frac{\partial u}{\partial y} = -\frac{\partial p}{\partial x} + \frac{\partial}{\partial y}\left(\mu_T \frac{\partial u}{\partial y}\right) \tag{5}$$

$$\rho u \frac{\partial H}{\partial x} + \rho v \frac{\partial H}{\partial y} = \frac{\partial}{\partial y}\left[\frac{k_T}{C_p}\frac{\partial H}{\partial y} + \left(\mu_T - \frac{k_T}{C_p}\right)\frac{\partial u^2/2}{\partial y}\right] , \tag{6}$$

where we have represented the effective viscosity and thermal conductivity as

$$\mu_T = \mu + \rho\varepsilon \tag{7}$$

$$k_T = k + \rho\varepsilon_H/Pr , \tag{8}$$

respectively. Then, by defining an effective Prandtl number,

$$Pr_T = \frac{\mu_T C_p}{k_T} = Pr\left[\frac{1 + \varepsilon/\nu}{1 + \varepsilon_H/\nu}\right] , \tag{9}$$

we can re-write the energy equation in its familiar laminar form;

$$\rho u \frac{\partial H}{\partial x} + \rho v \frac{\partial H}{\partial y} = \frac{\partial}{\partial y}\left[\frac{\mu_T}{Pr_T}\frac{\partial H}{\partial y} + \mu_T\left(1 - \frac{1}{Pr_T}\right)\frac{\partial u^2/2}{\partial y}\right] . \tag{10}$$

These equations can be reduced to similarity form by introducing the Levy-Lees transformation (Hayes and Probstein, 1959),

$$\xi(x) = \int_0 \rho_e \mu_e u_e r^2 dx \tag{11}$$

$$\eta(x,y) = \frac{u_e r}{\sqrt{2\xi}} \int_0 \rho dy \tag{12}$$

and defining the new independent variables,

$$F' = u/u_e \tag{13}$$

$$G = H/H_e \ . \tag{14}$$

The resulting similar form of the equations is,

$$\left[CF''\right]' + FF'' + \beta(G-F'^2) = 0 \tag{15}$$

$$\left[\frac{CG'}{Pr_T}\right]' + FG' + \frac{(\gamma-1)M_e^2}{1+\frac{\gamma-1}{2}M_e^2}\left[\left(1-\frac{1}{Pr_T}\right)CF'F''\right]' = 0 \tag{16}$$

where

$$C = \frac{\rho\mu}{\rho_e\mu_e}\left(1+\frac{\varepsilon}{\nu}\right) \ . \tag{17}$$

For our incompressible results, the eddy viscosity in the turbulent sublayer was expressed algebraically as,

$$\varepsilon = K_\varepsilon u_k k\left\{1 - e^{-Re_K/A^+}\right\} e^{-\beta_1(y/k)^2} \ , \tag{18}$$

where K_ε, A^+, and β_1 are constants. For the compressible variable property case, we retain this same expression, but after non-dimensionalizing as required in Eq. (17), it differs from the corresponding incompressible formula by a viscosity ratio. Thus, for compressible flow, we have,

$$\frac{\varepsilon}{\nu} = K_\varepsilon \frac{\nu_k}{\nu} Re_k \left\{1 - e^{-Re_K/A^+}\right\} e^{-\beta_1(y/k)^2} \ . \tag{19}$$

For the compressible flow calculations which have been made to date, the constants in Eq. (19) have been kept at the same values as were used in the incompressible solutions. The only additional constant which must be evaluated for the compressible case is the "turbulent" Prandtl number, Pr_T, which was set equal to unity. To summarize, the constants for the compressible case are,

$$K_\varepsilon = 0.1 \qquad \beta_1 = 1.0$$
$$A^+ = 40 \qquad Pr_T = 1.0 \tag{20}$$

Finally, the Sutherland viscosity law was used to specify the viscosity-temperature relation.

The results of some compressible, rough-wall solutions are given in Section 4.2.

3.3 Effects of Ablation on Transition

The effects of ablation on boundary layer transition have also been estimated from linear stability results, and are shown in Figs. 3 and 4. These predictions, which are for an incompressible boundary layer, are based on an approximation of the stability characteristics of the blown boundary layer which is analogous to the one which was used to predict the effects of roughness on transition. The mean velocity profile for a typical blown boundary layer is shown in Fig. 3. This profile is compared with two other "equivalent" profiles. In the first case, the Falkner-Skan profile, which has the same shape factor, $H, (=\delta^*/\theta)$ as the blown velocity profile, is shown. For the second case, the Falkner-Skan profile, which has the same shear stress at the wall, τ_w, is shown. In order to obtain transition predictions without the necessity of computing the stability properties of the blown profiles, their stability characteristics were assumed to be approximated, in turn, by each of these two "equivalent" profiles. This resulted in two approximations for the transition Reynolds number at each blowing rate. These results are shown in Fig. 4 in terms of the predicted transition Reynolds number as a function of the non-dimensional blowing rate, B', for each of three free-stream pressure gradients, namely, $\beta = 0$, $\beta = 0.2$, and $\beta = 0.5$. The $\beta = 0$ case corresponds to a flat plate, while the $\beta = 0.5$ case corresponds to the flow past an axisymmetric stagnation point. The solid lines represent the predicted transition Reynolds numbers based on the equivalent τ_w assumption. As can be

seen, both approximations give essentially the same predictions. These predictions indicate that blowing strongly decreases the transition Reynolds number for all three pressure gradient cases. It should be noted that a typical ablation rate for a re-entry nosetip corresponds to a blowing rate of about $B' = 0.5$ (or less). The predictions on this curve extend to much higher levels of wall mass-flux than are realistic in order to indicate the trends, and in order to bring the transition Reynolds number for the highly favorable pressure gradient case down to the level at which stability results were available. These predictions indicate that the levels of ablation which are encountered on a re-entry nosetip are enough to reduce the transition Reynolds number by about a factor of two from the smooth-wall, non-blown case. However, as noted below, blowing from a rough surface may give, qualitatively, the opposite effect (at least for small values of blowing). Finally, it should be noted that the flat plate and axisymmetric stagnation point cases were enputed for a Prandtl number, 0.7, and for a viscosity-temperature relation of the form, $u \propto T^{\omega}$, where $\omega = 0.7$. The $\beta = 0.2$ case was for a Prandtl number of unity in which the viscosity was taken to be proportional to the temperature.

3.4 Comparisons between Stability Theory Predictions and the Aerotherm Correlation

At this point, it is useful to compare the general form of the linear stability predictions with the transition correlation which was developed from the PANT series data by Anderson (1973). His correlation related the momentum thickness Reynolds number at transition to the surface roughness, and the wall-to-free-stream temperature ratio as,

$$Re_{\theta_{TR}} = 215 \left\{ \left(\frac{k}{\theta} \right)^{-1} T_w/T \right)^{0.7} . \qquad (21)$$

This correlation is for wind-tunnel data taken on non-ablating models, but it has since been modified (Anderson, 1975) by means of analytical arguments so that it will include the effects of ablation. Based upon an assumption that the "disturbance level" which exists inside the pre-transitional boundary layer is proportional to the kinetic energy of the flow at the top of the roughness element, Anderson extended the relation to the form

$$Re_{\theta_{TR}} = 215 \left\{ \left(\frac{k}{\theta}\right)^{-1} \left[\frac{B'}{10} + \left(1 + \frac{B'}{4}\right) \frac{\rho_e}{\rho_w} \right] \right\}^{0.7} , \qquad (22)$$

where the temperature ratio, T_w/T_e, has been replaced by the density ratio, ρ_e/ρ_w. For a perfect gas, these are, of course, identical, but for the non-perfect gas which exists near the surface of a re-entry vehicle, they can be considerably different. The argument that the disturbance level depends on the kinetic energy ratio suggests that it is the density ratio, not the temperature ratio, that is important in the transition process.

In our roughness model, the effect of the roughness enters in two ways: through the roughness Reynolds number, $Re_k = u_k k/\nu$, and through the length ratio, k/δ_k, where δ_k represents some (unspecified) integral thickness of the boundary layer. That is to say, the roughness appears in two dimensionless forms: the characteristic boundary layer thickness, δ_k, and the length scale, ν_k/u_k. The kinetic energy ratio (which was used by Anderson) and the roughness Reynolds number are closely related. In particular, we can express the velocity, u_k, as

$$u_k \approx k \frac{\Delta u}{\Delta y} \approx k \frac{u_e}{\delta_k} . \qquad (23)$$

Then we have

$$Re_k = \frac{\rho_k u_k^2}{\rho_e u_e^2} Re_{\delta_k} (T_e/T_w)^{\omega} , \qquad (24)$$

where the viscosity ratio has been replaced by a temperature ratio. Thus, the two relations differ by a Reynolds number and a temperature ratio.

A qualitative comparison of the stability analysis and the transition criterion developed by Anderson is given in Table I. The table compares the predicted effects of roughness, blowing, blowing in combination with roughness, and pressure gradient. Both linear stability theory and the Aerotherm criterion predict that roughness has a strong effect on the transition Reynolds number. The Aerotherm criterion indicates that transition will never occur if the surface is perfectly smooth (*i.e.*, $Re_{TR} \to \infty$ as $k \to 0$). Our stability-based roughness model, in turn, indicates that there is a threshold roughness height below which roughness has no effect (or a negligible effect). Thus, in the

limit as $k \to 0$, stability theory predicts that the transition Reynolds number will approach a (finite) constant. Both of these behaviors suggest that, for smooth surfaces, phenomena in addition to roughness control the transition process. These additional phenomena have been (implicitly) included in the stability approach, but have been omitted in the Anderson calculations.

Because of its limitation to finite values of roughness, the Aerotherm criterion cannot be used to predict the effect of ablation (blowing) on a smooth surface. The stability results, as indicated above, predict that blowing has a strong de-stabilizing effect on the boundary layer; that is, blowing moves transition rapidly forward.

The combination of blowing in the presence of roughness behaves quite differently from blowing in conjunction with a smooth surface. The Aerotherm criterion indicates that blowing tends to diminish the effect of the surface roughness and causes transition to move backward (away from the stagnation point). Definitive results from the stability predictions have not been computed yet, but initial observations, based on qualitative comparison of the mean-flow profiles, indicate that the stability results will also predict an initial increase in the transition Reynolds number for mild amounts of blowing. If the blowing rate is increased to successively higher values, it will eventually control the transition location and cause it to move forward once again. Thus, the stability analysis indicates that there will be a roughness-dominated regime in which increased ablation stabilizes the boundary layer and causes the transition location to move backward; there will also be a blowing-dominated regime in which increased ablation destabilizes the boundary layer.

4. STABILITY CALCULATIONS

Although we have been able to use existing stability calculations which have been reported in the literature to obtain some stability-based transition predictions, and to determine the relative importance of some parameters in controlling the transition location, it is still imperative that we generate additional stability calculations to enable us to investigate the complete spectrum of mechanisms which can affect the nosetip boundary layer. In order to obtain the capability for computing these required results, we have acquired a copy of the linear stability code which has been developed by Mack (1974) at JPL over the past decade. Our version of this program is complete, and is in a "production" state. The program will compute the stability properties of either

two-dimensional or three-dimensional (skewed waves) disturbances in a boundary layer. It solves the complete, viscous stability equations for either compressible or incompressible flows and, in addition to being capable of handling two-dimensional mean flows, it can also handle three-dimensional boundary layers.

Our version of this computer program has been carefully verified on a number-to-number vasis against appropriate test cases which were supplied by Mack to ensure that all machine-to-machine incompatibilities which were introduced by the required machine conversion were removed. Following this, the code was checked against the incompressible tabulations of Wazzan, Okamura and Smith (1968) to ensure that our version of Mack's code gave results which were identical to those which had been obtained from other independent codes. To ensure maximum verification, our "incompressible" test cases were run at a Mach number of 0.01 so that the code was forced to use the compressible flow logic which was to be used for the cases of interest in the nosetip problem. This check also verified that the coupling between our mean-flow boundary layer program (similarity solution) and the stability program was proper. The results of both zero and non-zero pressure gradient calculations from our stability program proved to be identical to the results which were reported by Wazzan *et al.* (1968) (to the accuracy to which we could read their published curves).

Following the verification of the code, some minor modifications were made to adapt the code to our specific needs. The most significant modification was to add a control loop to the program which would allow the eigenvalues at a sequence of frequencies on a constant Reynolds number line to be computed in a single pass on the machine. In this mode, the computer stores previous eigenvalues and uses them to compute an accurate new guess for the eigenvalue at the next higher (or lower) frequency. Because of the improved initial guesses which can be obtained, this control loop not only decreases the number of person-hours which are required to compute a stability map, but it also decreases the amount of computer time which is required per eigenvalue. A parallel capability for computing the eigenvalues at a series of Reynolds numbers on a fixed frequency line was also included. In addition to incorporating this new control loop, a few other minor changes were made.

The stability computations which we have made with our code can be divided into two specific categories: a parametric series of calculations and some actual nosetip boundary layer calculations. These two types of calculations are discussed separately below.

4.1 Parametric Stability Calculations

The parametric stability calculations are being computed so that a data base of stability results will be available for use in making rapid, approximate estimates of the effects of various parameters on the transition location. These parametric solutions are to be used in a manner similar to that used for the incompressible, rough-wall transition predictions which were reported previously (Merkle, Kubota, and Ko, 1974) and for the effects of ablation which were described in Section 3 of the present Report. Of course, in the compressible boundary layer, a two-parameter family of solutions will have to be considered in order to include the important effects of heat transfer. Although sufficient data is still not available to make these approximate predictions, we anticipate that these two variables will be the shape factor, H (as was used for the incompressible results), and the wall-to-free-stream temperature ratio, T_w/T_e.

Since the transition location generally occurs within the subsonic portions of the nosetip boundary layer (Anderson, 1975), we have restricted our parametric stability tabulations to low Mach number regions. In particular, most of the results have been computed for a unity-Mach number boundary layer. A few results have also been tabulated at $M_e = 0.5$, but these results are to be used primarily to verify the accuracy of interpolation between the Mach-one results and the incompressible results (which have been reported by Wazzan *et al.*, 1968). At present, the adiabatic wall case has been computed for the similarity profiles of the Mach-one boundary layer for a range of favorable and non-favorable pressure gradient cases. The results show that even at these low Mach numbers, substantial compressibility effects appear in the stability solutions. For example, the maximum amplification rates for a specific value of the pressure gradient parameter in the Mach-one boundary layer are about half the corresponding value in the incompressible boundary layer. Similarly, the critical Reynolds numbers of the compressible boundary layer occur some twenty percent below their incompressible counterparts. A complete listing of the eigenvalues which we have computed for the Mach-one boundary layer are given in Table II. Some summary plots of the results are shown in Figs. 5 through 8.

Figure 5 shows neutral stability curves; that is, curves along which disturbance amplification rate is equal to zero, for flows with unity free-stream Mach number and pressure gradients ranging from highly adverse, $\beta = -0.1$, to quite favorable, $\beta = 0.2$, where β is the usual Falkner-Skan pressure gradient parameter. The neutral stability curve for a boundary layer near an axisymmetric stagnation point ($\beta = 0.5$) is given in Fig. 6b. As might be expected in the light of incompressible flow results, the stability characteristics are strongly affected by pressure gradient; the boundary-layer becomes increasingly stable as the magnitude of the favorable pressure gradient increases.

The effect of free-stream Mach number on boundary layer stability characteristics is indicated in Figs. 6a and 6b which show neutral stability curves for both incompressible and unity Mach number flows with $\beta = 0.1$, 0.2 and 0.5. The critical Reynolds numbers corresponding to the Mach-one cases are significantly smaller than those of the corresponding incompressible flows.

Neutral stability curves for disturbances in the form of oblique waves skewed at an angle, ψ, from the normal to the free-stream direction are shown in Fig. 7. For incompressible flow, Squire's theorem (*see* Rosenhead, 1963) states that the neutral stability curves when plotted in terms of the normalized variables, $\tilde{F} = F/\cos^2\psi$ and $\tilde{R} = R\cos\psi$ where $R = \sqrt{Re_x}$, will coincide for all wave angles. As a result, it follows that the most unstable wave, *i.e.*, the lowest critical Reynolds number, is the two-dimensional wave with $\psi = 0^\circ$. In contrast to this, Fig. 7 shows that the lowest critical (non-dimensionalized) Reynolds number in the Mach-one case corresponds to a 30° wave; Squire's theorem clearly does not hold at Mach one.

Figure 8 shows the disturbance amplification rate, α_i, normalized by $\cos\psi$ for a range of $\tilde{R}$ at a fixed value of $\tilde{F}$. Negative values of α_i represent growing and, hence, unstable waves. As noted above, normalized curves for various values of ψ will collapse onto a single line for an incompressible boundary layer. For the compressible case shown here, the normalized amplification rate, α_i, is greatest for a wave skewed at 60° to the free-stream direction, while the largest non-normalized amplification rate corresponds to the wave with $\psi = 30^\circ$. The maximum non-normalized amplification rate for a wave at 60° is substantially smaller than the corresponding rate at either 0° or 30°. This behavior is in agreement with the results of Mack (1969) who showed that the wave angle of the most unstable disturbance, in the sense of maximum amplification rate overall frequencies, increases rapidly with Mach number and is in the range from 55° to 60° for Mach numbers greater than 1.6.

If these tabulated results are to be used to compute parametric transition predictions, some type of interpolation must be devised to enable us to obtain rapid, accurate estimates of the eigenvalues at intermediate values of the parameters. If the eigenvalue at a specific Reynolds number and frequency is desired for a Mach-one boundary layer, it can be simply obtained by an interpolation. However, for intermediate Mach numbers, pressure gradients, *etc.*, a more difficult multiple interpolation is required. Using the Mach number interpolation as an example, the interpolation between the Mach-one results and the incompressible results is to be obtained from solutions which are stored in the non-dimensional form, Re/Re_{CR} vs. ω/ω_{CR}, where the subscript "CR" refers to the critical value. A comparison of the gradient parameter, $\beta = 0.5$, is shown in Fig. 9. As can be seen, these variables appear to be much more desirable for use in Mach number interpolation than do the original (Re,ω) variables (*see* Fig. 5).

4.2 Nosetip Stability Calculations

In addition to the parametric studies described above, some computations of the stability characteristics of the boundary layer on a nosetip have also been made. For these initial computations, a local similarity approximation was used to compute the mean flow profiles and to include the surface roughness effects. Additional computations, which will be based on a finite-difference solution of the boundary layer equations, are planned. These nosetip calculations combine the effects of all the individual parameters into a single computation. In particular, realistic values of roughness, wall-temperature, pressure gradient and local Reynolds number have been used. In order to determine the relative effects of the various parameters, some smooth-wall and some adiabatic-wall calculations have also been completed.

The values of the nosetip parameters which were used in the calculations have been taken from a SNAP computer output which was supplied to us by the Aerotherm Corporation. The computed properties are for a nosetip at an altitude of 59,000 feet, a free-stream Mach number, $M_\infty = 22.6$, and a free-stream total pressure of 50.7 atmospheres. The ablative nosetip radius was initially 1.5 inches, and for the conditions just described, it remains nearly unchanged in size and shape (hemispherical). Values of wall temperature, local total pressure, local pressure gradient and Mach number were obtained from the computer print-out. Corresponding integral boundary layer properties, including the

momentum thickness, θ, and the displacement thickness, δ^*, were also supplied to us by Aerotherm from their BLIMP boundary layer code. The roughness of the nosetip surface was estimated to be about 0.6 mils.

A plot which shows the variation in the Mach number at the boundary layer edge, the wall-to-free-stream temperature ratio, the static pressure distribution and the Reynolds number based on momentum thickness as a function of distance from the stagnation point is shown in Fig. 10. The static pressure variation in Fig. 10 has also been re-plotted in Fig. 11 in terms of the similar pressure gradient parameter, β, as defined in the Levy-Lees transformation. As can be seen in Fig. 11, the pressure gradient parameter, β, is nearly constant at the value of $\beta = 0.5$ for some distance, and then begins to increase somewhat. For reference, the pressure distribution as computed by modified Newtonian theory is also included in Fig. 11. Finally, it should be noted that the Aerotherm transition criterion (Anderson, 1975) indicated that transition would occur at about 0.7 inches downstream of the stagnation point.

The mean flow profiles were computed from the Levy-Lees transformed equations of motions (Hayes and Probstein, 1959). Effects of roughness were included by means of the compressible version of the turbulent sublayer model which was described in Section 3.2. Then, the similar profiles were computed and scaled to give the proper momentum thickness Reynolds number (as determined from the BLIMP calculation).

At the present time, stability characteristics have been computed at two points on the boundary. One point is at an arc-length distance of $S = 0.1$ in., which is near the stagnation point. The other point is at a location of $S = 0.7$ in., which is near the indicated transition location. At the first point, $S = 0.1$ in., the important parameters of interest have the following values: edge Mach number, $M_e = 0.09$; pressure gradient, $\beta = 0.50$; and wall temperature ratio, $T_w/T_e = 0.52$. A plot of the mean velocity distribution for the smooth wall case and a 0.3 mil roughness case is shown in Fig. 12. The computed Reynolds number based on the boundary layer thickness, δ (defined as the location where $u/u_e = 0.999$), is $Re_\delta = 155$. The roughness Reynolds number, Re_k, for this case is $Re_k = 20$. Because of this small value, the effect of the roughness on the stability properties at this location was quite small. As a result, our analysis showed that all disturbances which were introduced into the boundary layer were damped, even in the presence of roughness. As an indication of the margin of stability,

an approximate value of the critical Reynolds number was determined. For the present edge conditions, but with an adiabatic smooth wall, the critical Reynolds number is about Re_δ = 37,000. Computations for a smooth, cold wall were not made, but it is known that the smooth-wall boundary layer becomes more stable with cooling. Thus, it is expected that the smooth cold-wall critical Reynolds number will be above 37,000. Similar stability calculations for a rough, adiabatic wall case indicated a critical Reynolds number of about 13,000 based on boundary layer thickness. It is expected that the roughness is sufficiently large to lower this value somewhat as the wall is cooled to the indicated T_w/T_e = 0.52 conditions, but, again, a verification of the temperature effect was not made. It should be noted that these estimates of the critical Reynolds number are only approximate and are intended to demonstrate the excessive margin of stability which exists at this near-stagnation point location. Besides the stability of the boundary layer, the other important point to note is that the roughness, even at these low Reynolds numbers, decreases the critical Reynolds number by about a factor of three.

Additional computations of the stability characteristics of the boundary layer at a region very near the transition location (S = 0.7 in.) are currently in progress, but have not been completed as yet. The boundary layer edge conditions at this location are: M_e = 0.66, β = 0.63, and Re_δ = 595. Because of the higher local Reynolds number at this point in the boundary layer, the roughness Reynolds number, Re_k, is also larger and is expected to have a more dominant effect. The computed value of Re_k is about 150. For the adiabatic smooth-wall case, the critical Reynolds number is around 40,000, which is somewhat different than the S = 0.1 case described above because of the difference in the Mach number and pressure gradient. Again, cold-wall values are expected to be somewhat larger. The corresponding stability maps for the rough-wall cases have not been completed yet. Thus, at the present time, it is uncertain as to whether or not the combined effects of roughness and cooling will decrease the critical Reynolds number to a value below the expected transition Reynolds number. The above figures indicate that roughness has to decrease the critical Reynolds number by a factor of 100 in order for stability theory to be able to predict transition at the correct position. Comparisons between rough and smooth surfaced nosetips suggest that roughness can easily have an effect which is this strong (*see* discussion in the next Section).

Without the aid of the final rough-wall nosetip calculations, it is difficult to speculate on the outcome of the predictions; however, a few philosophical points are in order. If the current roughness model does not lower the critical Reynolds number sufficiently to enable transition to be predicted at the Reynolds numbers which have been observed experimentally, this can be easily rectified by an appropriate change in the values of the constants in the turbulent sublayer model. That is to say, we could choose to evaluate the constants in the roughness model on the basis of nosetip experiments, not flat plate data as has been originally used. We prefer, however, to view the roughness constants as being fixed. Consequently, if this conjectured inability to predict nosetip transition does occur, we prefer to return to the equations of motion and carefully re-evaluate the terms which have been neglected in an attempt to find specific effects which can substantially affect the stability characteristics on the nosetip.

5. ADDITIONAL TRANSITION MECHANISMS

The success (or failure) of any theoretical procedure for the prediction of transition on a rough nosetip is tempered by the fact that in including the effects of surface roughness, some empirically determined constants must be introduced in addition to those which are required for the prediction of transition on smooth walls. Thus, a "proper" choice of the constants will always allow the correct transition location to be predicted, or at least, the theory can be "tuned" by evaluating the constants from one series of experimental data and then using it to predict other similar series. Although such a procedure can and must be used to some extent to describe a process as complex as the nosetip transition phenomena, it tends to obscure the question of whether or not the proper mechanisms are being simulated. One way to verify more fully the mechanisms which lead to transition is to use the theory to predict nosetip transition in situations in which surface roughness is not a factor, *i.e.*, to consider smooth-wall nosetip transition. Then, if proper transition mechanisms can be predicted for the smooth-walled case (for which a theoretical model would require a minimal amount of empiricism), the rough-wall predictions can be accepted with more confidence. Unfortunately, this strategy leads to other complications since new mechanisms take over when roughness is eliminated. Nevertheless, it is useful to consider the transition locations which have been observed on smooth-walled nosetips.

5.1 Experimental "Smooth-Wall" Nosetip Transition

Since it is impossible to obtain a surface which is "smooth" in the mathematical sense, we will use the term "smooth" to refer to a surface whose roughness has a negligible effect on the location of transition. Unfortunately, the experimental data do not show any clear-cut level below which the wall-roughness ceases to affect transition. However, a number of transition tests on highly polished surfaces have been reported. Garland and Chauvin (1957) reported transition Reynolds numbers (based on momentum thickness) of between 160 to 600 for an 8-inch diameter sphere-cylinder whose surface was polished to a finish of less than 25 microinches of roughness. These transition measurements were obtained in free-flight experiments at Mach numbers between 2.0 and 4.0, and at wall-to-free-stream temperature ratios of about T_w/T_e = 1.0 - 1.2. In comparison with the 25 microinch surface roughness, the laminar boundary momentum thickness on the nosetip was on the order of one mil. Tests of a hemisphere-cone at similar flight conditions (Chauvin and Speegle, 1957) and with a similar 25 microinch roughness on the nosetip showed similar nosetip transition Reynolds numbers (Re_θ = 300 - 400). In view of the small value of the ratio of surface roughness to boundary layer thickness on these models, the surface roughness would not be expected to have an important effect on the transition location; however, the results of a second series of tests with even smoother nosetips indicates that this is not true. Buglia (1957) and Hall, Speegle, and Piland (1957) tested nosetips whose surface roughness was about 5 microinches. Their results indicated that transition on the 5 microinch nosetip occurred at Reynolds numbers which were about a factor of four higher than the corresponding 25 microinch results. For the 5 microinch nosetip, transition Reynolds numbers of from 800 to 2,200 on a sphere-cylinder and from 900 to 1,200 for the sphere-cone, respectively, were observed. Thus, it appears that even for these highly polished surfaces, the roughness exerts a significant control over the transition location.

Additional evidence of the sensitivity of the location of transition to the surface finish on the nosetip was reported by Dunlap and Kuethe (1962). They observed nosetip transition Reynolds numbers which were around Re_θ = 600 for a ratio of surface to free-stream temperatures ranging from T_w/T_e = 0.5 to T_w/T_e = 1.2, in a simulated hypersonic environment. Their results were for a "very highly polished" surface ("probably around a few microinches of roughness"), but they noted that dust particles tended to collect near the stagnation

point (within 10 degrees) and cause premature transition. Meaningful data could only be obtained by frequent polishing and inspection of the nosetip for dust accumulation, pitting, and frost due to freezing of CO_2. Thus, the experimental determination of the transition location on a smooth nosetip may not only be sensitive to how smooth the nosetip is, but also to the care with which the experiment is conducted. In tests in which very highly polished surfaces are used, the experimental conditions must be extremely closely monitored to ensure unambiguous results.

5.2 Additional Transition Mechanisms and Possible Extension of Stability Theory

Stability theory indicates that the critical Reynolds number in axisymmetric boundary layer near a stagnation point occurs at a value of $Re_\theta = 3,300$, which is considerably higher than the transition Reynolds numbers which are quoted above for highly polished surfaces. Whether or not transition on a completely smooth surface would occur at Reynolds numbers which are above this value remains an open question. Consequently, it is imperative to review the known theoretical arguments for other potential transition mechanisms in an attempt to ascertain their effect on nosetip transition. Thus, we approach the problem from the following viewpoint. Transition is experimentally observed to occur on the nosetip in regions where classical parallel flow stability theory (without the aid of a roughness model) indicates that all disturbances are damped. If transition, in fact, does occur as a result of the growth of small disturbances, some other physical phenomena which have been hitherto ignored must be included in the problem formulation. Specifically, some terms in the stability equations, which have been assumed to be of higher order and ignored, may in reality have a significant effect. One path around this dilemma is through the use of a roughness model which affects the mean velocity profiles. However, this roughness analysis can, at most, be included in an approximate way, and it must include empirical "constants". To be sure, these constants can easily be adjusted so that instability and transition are predicted to occur on the nosetip, but such an arbitrary adjustment of constants in order to match the experimental data has little meaning, especially if we are interested in elucidating the mechanisms which lead to nosetip transition. An alternative approach is to review carefully the ordering of terms in the linearization and simplification of the stability equation to determine which (if any) effects have been inadvertently relegated to higher order and, hence, dropped from the analysis, despite their first-order effect in the physical situation. Some of the effects

which have been neglected in our current analysis are:

1. Effects of streamline curvature in the approach to the stagnation point which could lead to Taylor-Görtler (longitudinal) instability;
2. Additional axisymmetric terms in the equations of motion;
3. Coupling between disturbances and the mean flow profiles (even in regions where disturbances are damped) which act in a cumulative sense alter the mean-flow profiles and, hence, alter the stability characteristics;
4. Unsteadiness in the mean flow caused by "wandering" of the stagnation point;
5. Effects of non-zero velocity gradients (rotational flow) outside the boundary layer caused by entropy swallowing effects.

A brief review of these supposedly "higher order" influences is given below.

Some evidence of the importance of Görtler instabilities, or axisymmetric vortex stretching effects was reported by Kuethe (1957), who observed the growth of wave-like disturbances in the boundary layer over a hemisphere at local Reynolds numbers which were substantially below the critical value. Motivated by these observations, he performed a simple analysis which indicated that the vortex stretching effects, which occur as the fluid in the boundary layer is swept over the sphere, are responsible for the observed amplification. His model is, however, essentially a dimensional analysis, and cannot by itself yield quantitative results. Kuethe's analysis suggests that the stretching of a longitudinal vortex in a region in which the velocity gradient, $\partial u/\partial x$, is constant is given by

$$v_2'/v_1' = \sqrt{x_2/x_1} \quad ,$$

where x_1 represents the position of a particle in the boundary layer at some initial time, and x_2 represents its position an incremental time later. v_2 and v_1 are the corresponding disturbance velocities. A similar analysis for the stretching of an aximuthal vortex filament, corresponding to an axisymmetric Tollmien-Schlichting wave (which was suggested, but not carried out by Kuethe) gives,

$$v_2'/v_1' = \sqrt{R_2/R_1} \quad ,$$

where R represents the radial coordinate of the sphere. A quantitative evaluation of these vortex stretching mechanisms would require either an analysis of the complete Görtler instability equations (for the former case) or of the axisymmetric form of the Tollmien-Schlichting equations (for the latter case). An assessment of the feasibility of such an analysis is currently underway.

The inclusion of the coupling and the cumulative interaction between the disturbances and the mean flow could be easily incorporated into a stability analysis if only single frequency disturbances were considered. Thus, if a disturbance/mean flow energy transfer were allowed, the disturbances would feed energy into the mean flow as they decayed (in the stable region), and, as a consequence, the mean flow profiles would become distorted. These distorted profiles could, in turn, generate an instability; however, the likelihood of such a process being significant seems remote.

Unsteadiness in the mean flow profiles has been reported by Kuethe, Willmarth, and Crocker (1960), who described experimental evidence of random fluctuations or "wandering" of the stagnation point about its equilibrium position on hemispherical wind-tunnel models in both subsonic and supersonic free-stream flows. Similar observations have also been reported by Peterson and Horton (1959). A Görtler-like stagnation point instability (*see above*) and stretching of vortex filament in the diverging stagnation point flow were suggested as possible generation mechanisms for these mean flow fluctuations. Such stagnation point "wandering" would clearly lead to mean flow fluctuations which have not been considered in the present study.

The strongly curved, hypersonic bow shock causes an inviscid shear flow layer to be generated in the region outside the boundary layer. In all of our calculations to date, this shear layer has been ignored, and the flow outside the boundary layer has been taken as being uniform and parallel. The inclusion of the characteristics of this shear layer in the stability solutions could be accomplished by simply extending the mean flow profiles which are used in the stability calculation beyond the "edge" of the boundary layer. Again, order-of-magnitude estimates of the effect of this shear layer suggest that it is not sufficiently strong to materially affect the stability characteristics; however, a more rigorous analysis may be justifiable.

5.3 Comparison with Turbulent-Modeling Approaches

In conjunction with the above discussion, it should be pointed out that several of the items in the list of effects which are omitted in the stability approach are included in the turbulence-modeling approaches which are being used to predict transition (*see* Section 2.2). For example, the turbulence-modeling approaches do include the energy exchange between the disturbances and the mean flow. Nevertheless, it appears that the energy loss from the mean flow to the disturbances is not a significant effect until after the disturbances have grown quite large. That is to say, it appears that the initial growth of "turbulence", as computed by these models, would not be affected if the energy exchange between the mean flow and the turbulence were neglected. Thus, we believe that this effect which is included in the turbulence models and is ignored in the stability approach is not important. This speculation could be checked for the turbulence models by means of two back-to-back computations, the first of which would monitor the initial stages of the growth of the turbulence in a standard computation, while the second would monitor the turbulence growth in a computation with the coupling term "unhooked" from the mean flow, to determine the downstream location at which the two turbulence growth rates began to deviate from each other.

A second difference between the stability technique and the turbulence model approaches is that the latter include the full axisymmetric effects. This could be significant, especially very near the stagnation point where the axisymmetric terms dominate. As indicated above, an assessment of the importance of these effects and means of including them in the stability equations is currently being undertaken.

The longitudinal (Görtler) vortex effect represents a three-dimensional (*i.e.*, a variation with azimuthal angle, ϕ) effect which is ignored in both approaches. One deduction is that if it is not included in the turbulence model approaches, and if they can accurately predict nosetip transition, then, by implication, it is not important in the stability analysis either. This supposition, however, presupposes that the turbulence models predict transition at the right position for the right reason; in view of the large number of empirical constants involved, such is probably not a justifiable conclusion. We believe these 3-D effects could still be important, perhaps in a manner which is analogous to the observed spanwise variations which were observed in planar boundary layers, as discussed in Section 2.

Finally, it should be noted that stability theory includes some effects which the turbulence models ignore. One primary difference is that stability theory solves the complete time-dependent equations for the disturbances, whereas the turbulence model approaches include only the time-averaged equations. Of course, the dominant difference is that stability theory solves the actual equations of motion while the turbulence models solve a set of equations which "model" the equations of motion. In addition, these "models" have been developed for turbulence, not for the very different type of unsteadiness which characterizes the transitional boundary layer.

Another item of interest in the comparison between the two techniques is their treatment of the "production" and "dissipation" of disturbances. In stability theory, the growth (or decay) rate of disturbances is very much dependent upon their frequency content, and the amplification rate for the unstable frequencies is strongly affected by the existence of a point of inflection in the boundary layer profile. Thus, for example, if we consider the family of Falkner-Skan profiles, the favorable pressure gradient cases, which have no point of inflection, become increasingly stable to small disturbances as the pressure gradient parameter is increased. By way of contrast, the unfavorable pressure gradient cases have a point of inflection which moves steadily away from the wall as the value of β get more negative, and, correspondingly, the amplification gets increasingly more rapid. Turbulence models, however, generally have a production term which depends on the magnitude of the velocity gradient. This suggests that steep velocity gradients (such as occur in fully turbulent boundary layers or favorable pressure gradient, laminar boundary layers) increase the production of turbulence. Thus, it appears that a favorable pressure gradient (positive value of β) would lead to increased production, whereas an unfavorable pressure gradient would decrease the production of turbulence. Of course, the net change of turbulence must include the dissipative effects also, and it is the balance between these two terms which yields the net growth rate of the disturbances in the laminar boundary layer.

6. SUMMARY AND CONCLUSIONS

Linear stability theory has been used as the basic theoretical foundation for an analysis of the mechanisms which lead to boundary layer transition on the nosetip of a re-entry vehicle. In this analysis, the effects of surface roughness, wall cooling, ablation, pressure gradient, and axisymmetric geometry have been considered both individually and in combination with each other. The results suggest that surface roughness is an important controlling parameter in determining the location of transition, but that the other parameters can substantially alter the "effective" roughness height.

Some specific observations and conclusions which can be made regarding nosetip transition include:

1. A number of physical processes, which have a profound influence on the location of transition, occur prior to the "beginning" of the transition region as it is microscopically observed. The use of linear stability theory in a technique for predicting transition is attractive because it includes the capability for faithfully predicting these pre-transitional phenomena;

2. Nosetip transition is experimentally observed to occur at local Reynolds numbers which are substantially smaller than the critical value which is predicted by stability theory. Consequently, classical, parallel-flow stability results, without modification, are unable to explain these experimental transition locations (however, *see* Item 3 following);

3. The effects of surface roughness have been included in the stability analyses of nosetip boundary layers by means of a "turbulent sublayer" model which alters the mean flow profiles and reduces the critical Reynolds number sufficiently to allow the application of stability theory in nosetip-like environments. Some specific predictions of the roughness model are:

   a. Experimentally observed effects of roughness on transition can be predicted.

   b. The effect of cooling a rough surface tends to destabilize the boundary layer and cause earlier transition (because the boundary layer thinning effect which is caused by cooling makes the roughness more effective). By contrast, cooling a smooth wall makes the bounday [illegible] more stable.

c. The effects of ablation on a smooth-wall boundary layer are to decrease the transition Reynolds number. Preliminary results indicate that ablation, in combination with rough surfaces, can, again, have the opposite (*i.e.*, stabilizing) effect;

d. Sufficiently large roughnesses can essentially negate the strongly stabilizing effect of highly favorable pressure gradients such as the ones which occur in the nosetip region;

4. The effects of wind-tunnel Re/in. on the transition Reynolds number have been investigated, but it appears that the frequency content of the free-stream disturbances must be included before this effect can be properly predicted;

5. An extensive tabulation of the stability characteristics of a Mach-one boundary layer (for both favorable and unfavorable pressure gradients) has been compiled and is presented herein. These results show that, even at unity Mach number, compressibility has a significant effect on the stability characteristics;

6. Computations of the stability properties of an actual nosetip boundary layer have indicated that regions near the stagnation point are stable to all disturbances, even in the presence of roughness. Analyses further away from the nosetip are currently in progress;

7. A number of additional factors which could influence the growth of disturbances in the nosetip boundary layer, but which have until now been ignored in the stability analysis, have been identified and are being more carefully evaluated.

REFERENCES

Anderson, A. D. (1975) "Boundary Layer Transition on Nosetips with Rough Surfaces", "Appendix A," Aerotherm Corp., Mountain View, CA.

Anderson, A. D. (1974) "Passive Nosetip Technology (PANT) Interim Report, Vol. III, Surface Roughness Effects, Part III, Transition Data Correlation and Analysis," Aerotherm Report 74-90, Aerotherm Corp., Mountain View, CA (*CONFIDENTIAL*).

Anderson, A. D. (1973) "Analysis of PANT Series A Rough Wall Calorimeter Data, Part II: Surface Roughness Effects on Boundary Layer Transition," Aerotherm Report 73-81, Aerotherm Corp., Mountain View, CA.

Beckwith, J. E., Bushnell, D. M. (1968) "Detailed Description and Results of a Method for Computing Mean and Fluctuating Quantities in Turbulent Boundary Layers," NASA TN D-4185.

Buglia, J. J. (1957) "Heat Transfer and Boundary Layer Transition on a Highly Polished Hemisphere-Cone in Free Flight," NASA TN D-955.

Chauvin, L. T. and Speegle, K. C. (1957) "Boundary Layer Transition and Heat Transfer Measurements from Flight Tests of Blunt and Sharp 50° Cones at M_∞ = 1." to 4.7," NACA RM L57D04.

Donaldson, C., DuP. (1969) "A Computer Study of an Analytical Model of Boundary Layer Transition," *AIAA J.*, Vol. 7, No. 2, p.271.

Dunlap, R. and Kuethe, A. M. (1962) "Effects of Cooling on Boundary Layer Transition on a Hemisphere in Simulated Hypersonic Flow," *J. Aero. Sciences*, Vol. 29, No. 12, p. 1454.

Dryden, H. L. (1959) *Aerodynamics and Jet Propulsion*, Vol. 3, Princeton University Press, Princeton, NJ.

Finson, M. L., Lewis, P. F., Wu, P. K. S., Teare, J. D., Pirri, A. N., and Nevolsine, P. E. (1974) "Advances Reentry Aeromechanics, Interim Scientific Report," PSI TR-10, Physical Sciences, Inc., Wakefield, MA.

Garland, B. J. and Chauvin, L. T. (1957) "Measurement of Heat Transfer and Boundary Layer Transition on an 8-Inch Diameter Hemisphere-Cylinder in Free-Flight," NACA RM L57D04a.

Grosch, C. E. (1974) "Predicting Transition from Laminar to Turbulent Boundary Layer Flow," Report, Old Dominion University Research Foundation, Old Dominion University, Norfolk, VA.

Hall, J. R., Speegle, K. C., and Piland, R. O. (1957) "Preliminary Results from Free-Flight Investigations of Boundary Layer Transition and Heat Transfer on a Highly Polished Hemisphere-Cylinder in Free-Flight," NACA RM L57D18c.

REFERENCES (*cont'd*)

Hayes, W. D. and Probstein, R. F. (1959) *Hypersonic Flow Theory*, Academic Press, New York.

Kleganoff, P. S. and Tidstrom, K. D. (1972) "Mechanism by which a Two-Dimensional Roughness Element Induces Boundary Layer Transition," *Phys. Fluids*, Vol. 15, No. 7, pp. 1173-1188.

Klebanoff, P. S., Tidstrom, K. D., and Sargent, L. M. (1962) "The Three-Dimensional Nature of Boundary Layer Instability," *J. Fl. Mech.*, Vol. 12, p. 1.

Kuethe, A. M. (1957) "On the Stability of Flow in the Boundary Layer near the Nose of a Blunt Body," Report RM-1972, Rand Corp., Santa Monica, CA.

Kuethe, A. M., Willmarth, W. W., and Crocker, G. H. (1960) "Stagnation Point Fluctuations on Bodies of Revolution with Hemispherical Noses," Report No. MICH. 2753-2-F, Univ. of Michigan, Ann Arbor, MI.

Laufer, J. (1964) "Some Statistical Properties of the Pressure Field Radiated by a Turbulent Boundary Layer," *Phys. Fluids*, Vol. 7, No. 8, p. 1191.

Mack, L. M. (1975) "A Numerical Method for the Prediction of High-Speed Boundary Layer Transition using Linear Theory," Presentation given at NASA Conference on Aerodynamic Analyses Requiring Advanced Computers, Held at Langley Research Center, Hampton, VA.

Mack, L. M. (1974) "On the Application of Linear Stability Theory to the Problem of Supersonic Boundary Layer Transition," AIAA Paper 74-134. *See also AIAA J.*, Vol. 13, No. 3, p. 278.

Mack, L. M. (1971) "Progress in Compressible Boundary Layer Stability Computations," *Proceedings of the Boundary Layer Transition Workshop*, Vol. IV, Aerospace Corp., San Bernardino, CA.

Mack, L. M. (1969) "Boundary Layer Stability Theory," Report 900-277, Rev. A, Jet Propulsion Laboratory, Pasadena, CA.

Mellor, G. and Herring, H. J. (1972) "Computer Program for Calculating Laminar and Turbulent Boundary-Layer Development in Compressible Flow," NASA CR-2068.

Merkle, C. L., Ko, D. R. S., and Kubota, T. (1974) "The Effect of Axisymmetric Geometry on Boundary Layer Transition as Predicted by Linear Stability Theory," Research Report No. 39, Flow Research, Inc., Kent, WA (*also*, AFOSR-TR-75-0192).

Merkle, C. L., Kubota, T., and Ko, D. R. S. (1974) "An Analytical Study of the Effects of Surface Roughness on Boundary Layer Transition," Research Report No. 40, Flow Research, Inc., Kent, WA (*also*, AFOSR-TR-75-0190).

Orszag, S. A. (1974) "Numerical Simulation of Boundary Layer Transition on a Flat Plate," Research Report No. 33, Flow Research, Inc., Kent, WA.

Pate, S. R. (1971) "Measurements and Correlations of Transition Reynolds Numbers on Sharp Slender Cones at High Speeds," *AIAA J.*, Vol. 9, No. 6, p. 1082.

Pate, S. R. and Schueler, C. J. (1969) "Radiated Aerodynamic Noise Effects on Boundary Layer Transition in Supersonic and Hypersonic Wind Tunnels," *AIAA J.*, Vol. 7, No. 3, p. 450.

Peterson, J. B. and Horton, E. A. (1959) "An Investigation of the Effect of Highly Favorable Pressure Gradient on Boundary Layer Transition," NASA Memo 2-8-591.

Powars, C. A. (1973) "Analysis of PANT Series A Rough Wall Calorimeter Data, Part I: Surface Roughness Effects on Heat Transfer," Report 73-80, Aerotherm Corp., Mountain View, CA.

Rosenhead, L. (1963) *Laminar Boundary Layers*, Clarendon Press, Oxford.

Schubauer, G. B. and Klebanoff, P. S. (1956) "Contribution on the Mechanics of Boundary Layer Transition," NACA TR 1289.

Schubauer, G. B. and Skramstad, H. K. (1948) "Laminar Boundary Layer Oscillations and Transition on a Flat Plate," NACA TR 909.

Smith, A. M. O. and Gamberoni, N. (1956) Report ES-26388, Douglas Aircraft Company, Long Beach, CA.

Spangler, J. G. and Wells, C. J., Jr. (1968) "Effect of Free-Stream Disturbances on Boundary Layer Transition," *AIAA J.*, Vol. 6, p. 543.

Wazzan, A. R., Okamura, T. T., and Smith, A. M. O. (1968) "Spatial and Temporal Stability Charts for the Falkner-Skan Boundary Layer Profiles," Report No. DAC-67086, Douglas Aircraft Company, Long Beach, CA.

White, C. (1974) "Philco Transition Studies," Presentation given at Boundary Layer Transition and Shape Change Interchange Meeting III., held at Aerospace Corp., El Segundo, CA.

Wilcox, D. C. (1974) "Turbulence-Model Transition Predictions for Blunt-Body Flows," DCW-R-03-01 (*also*, AFOSR-TR-74-1714), DCW Industries, Sherman Oaks, CA.

TABLE I. COMPARISON BETWEEN AEROTHERM CRITERION AND L.S.T.

EFFECTS OF	L.S.T.	AEROTHERM
ROUGHNESS	STRONG DE-STABILIZING EFFECT ABOVE A PARTICULAR ROUGHNESS HEIGHT	STRONG DE-STABILIZING EFFECT
BLOWING	STRONG DE-STABILIZING EFFECT	
BLOWING IN COMBINATION WITH ROUGHNESS	MILD BLOWING TENDS TO DIMINISH EFFECT OF ROUGHNESS (ROUGHNESS DOMINATED) BUT STRONGER BLOWING DE-STABILIZES BOUNDARY LAYER (BLOWING DOMINATED)	BLOWING TENDS TO DIMINISH EFFECT OF ROUGHNESS-STABILIZES BOUNDARY LAYER
PRESSURE GRADIENT	LEVEL OF DP/DX AFFECTS TRANSITION MECHANISMS; VARIATIONS IN DP/DX LESS IMPORTANT.	NOT INCLUDED

TABLE 2: Tabulation of Linear Stability Computations

The following Table presents both real and imaginary wave number components computed at various values of Reynolds number and disturbance frequency for adiabatic boundary-layer flow at Mach one. Results are given for both adverse and favorable free-stream pressure gradients.

Definitions of Symbols Appearing in the Table

BETA	Falkner-Skan pressure gradient parameter.
MACH NO.	Free-stream turbulence.
TWALL	Wall temperature.
TSTAR	Free-stream total temperature.
R	Square root of Reynolds number based on x, $\sqrt{Re_x}$.
FR	Non-dimensional frequency, $\nu\omega/u_e^2$.
AR	Real part of the non-dimensional wave number, $\alpha = \sqrt{\frac{\nu_x}{u_e}}$.
AI	Imaginary part of the non-dimensional wave number, $\alpha = \sqrt{\frac{\nu_x}{u_e}}$.

MACH NO. = 1.0 BETA = .1
TWALL =300.00 TSTAR =250.00

R	FR	AR	AI
200.	.493E-04	.323E-01	.581E-02
200.	.781E-04	.449E-01	.353E-02
200.	.124E-03	.630E-01	.456E-03
200.	.156E-03	.751E-01	-.141E-02
200.	.196E-03	.900E-01	-.336E-02
200.	.220E-03	.987E-01	-.428E-02
200.	.220E-03	.987E-01	-.428E-02
200.	.247E-03	.108E+00	-.507E-02
200.	.311E-03	.131E+00	-.594E-02
200.	.391E-03	.159E+00	-.496E-02
200.	.493E-03	.192E+00	-.692E-03
250.	.220E-03	.120E+00	-.681E-02
300.	.250E-04	.267E-01	.431E-02
300.	.220E-03	.142E+00	-.654E-02
350.	.220E-03	.161E+00	-.376E-02
375.	.220E-03	.170E+00	-.191E-02
400.	.250E-04	.328E-01	.174E-02
400.	.281E-04	.357E-01	.120E-02
400.	.353E-04	.422E-01	-.727E-04
400.	.445E-04	.500E-01	-.160E-02
400.	.560E-04	.597E-01	-.336E-02
400.	.705E-04	.716E-01	-.521E-02
400.	.887E-04	.863E-01	-.689E-02
400.	.112E-03	.104E+00	-.788E-02
400.	.141E-03	.126E+00	-.742E-02
400.	.177E-03	.152E+00	-.468E-02
500.	.250E-04	.387E-01	-.406E-03
600.	.141E-04	.292E-01	.819E-03
600.	.177E-04	.345E-01	-.271E-03
600.	.223E-04	.409E-01	-.161E-02
600.	.250E-04	.446E-01	-.237E-02
600.	.250E-04	.446E-01	-.237E-02
600.	.281E-04	.487E-01	-.319E-02
600.	.353E-04	.583E-01	-.492E-02
600.	.445E-04	.701E-01	-.660E-02
600.	.560E-04	.847E-01	-.786E-02
600.	.705E-04	.102E+00	-.813E-02
600.	.887E-04	.123E+00	-.678E-02
600.	.112E-03	.146E+00	-.384E-02
600.	.141E-03	.172E+00	-.383E-03
700.	.250E-04	.505E-01	-.413E-02
800.	.887E-05	.259E-01	.549E-03
800.	.112E-04	.306E-01	-.451E-03
800.	.141E-04	.362E-01	-.169E-02
800.	.177E-04	.431E-01	-.316E-02
800.	.223E-04	.516E-01	-.479E-02
800.	.250E-04	.566E-01	-.561E-02
800.	.250E-04	.566E-01	-.561E-02

MACH NO. = 1.0 BETA = .1
TWALL =300.00 TSTAR =250.00

R	FR	AR	AI
800.	.281E-04	.621E-01	-.639E-02
800.	.353E-04	.749E-01	-.766E-02
800.	.445E-04	.904E-01	-.811E-02
800.	.560E-04	.108E+00	-.722E-02
800.	.705E-04	.129E+00	-.512E-02
800.	.887E-04	.152E+00	-.269E-02
800.	.141E-03	.212E+00	.489E-02
900.	.250E-04	.627E-01	-.674E-02
1000.	.445E-05	.185E-01	.141E-02
1000.	.705E-05	.258E-01	-.899E-04
1000.	.887E-05	.306E-01	-.115E-02
1000.	.112E-04	.363E-01	-.244E-02
1000.	.141E-04	.434E-01	-.393E-02
1000.	.177E-04	.520E-01	-.549E-02
1000.	.223E-04	.627E-01	-.692E-02
1000.	.250E-04	.688E-01	-.747E-02
1000.	.250E-04	.688E-01	-.747E-02
1000.	.281E-04	.756E-01	-.783E-02
1000.	.353E-04	.909E-01	-.777E-02
1000.	.445E-04	.108E+00	-.653E-02
1000.	.560E-04	.128E+00	-.475E-02
1000.	.705E-04	.151E+00	-.285E-02
1000.	.112E-03	.211E+00	.469E-02
1000.	.177E-03	.296E+00	.213E-01
1100.	.250E-04	.748E-01	-.779E-02
1200.	.281E-05	.152E-01	.162E-02
1200.	.445E-05	.212E-01	.441E-03
1200.	.560E-05	.250E-01	-.403E-03
1200.	.705E-05	.297E-01	-.147E-02
1200.	.887E-05	.353E-01	-.275E-02
1200.	.112E-04	.422E-01	-.420E-02
1200.	.141E-04	.507E-01	-.569E-02
1200.	.177E-04	.610E-01	-.699E-02
1200.	.223E-04	.736E-01	-.772E-02
1200.	.250E-04	.806E-01	-.774E-02
1200.	.250E-04	.806E-01	-.774E-02
1200.	.250E-04	.806E-01	-.774E-02
1200.	.281E-04	.882E-01	-.749E-02
1200.	.353E-04	.105E+00	-.632E-02
1200.	.445E-04	.123E+00	-.495E-02
1200.	.560E-04	.146E+00	-.338E-02
1200.	.705E-04	.172E+00	-.764E-03
1200.	.887E-04	.204E+00	.354E-02
1200.	.141E-03	.286E+00	.190E-01
1300.	.250E-04	.861E-01	-.740E-02
1400.	.353E-05	.201E-01	.320E-03
1400.	.445E-05	.238E-01	-.497E-03
1400.	.560E-05	.282E-01	-.153E-02

MACH NO. = 1.0 BETA = .01
TWALL =300.00 TSTAR =250.00

R	FR	AR	AI
1400.	.705E-05	.335E-01	-.277E-02
1400.	.887E-05	.401E-01	-.417E-02
1400.	.112E-04	.481E-01	-.560E-02
1400.	.141E-04	.580E-01	-.684E-02
1400.	.177E-04	.699E-01	-.754E-02
1400.	.223E-04	.836E-01	-.734E-02
1400.	.250E-04	.912E-01	-.690E-02
1400.	.250E-04	.912E-01	-.690E-02
1400.	.281E-04	.991E-01	-.636E-02
1400.	.353E-04	.117E+00	-.529E-02
1400.	.445E-04	.138E+00	-.403E-02
1400.	.560E-04	.163E+00	-.182E-02
1400.	.887E-04	.228E+00	.755E-02
1500.	.250E-04	.959E-01	-.642E-02
1550.	.250E-04	.982E-01	-.621E-02
1600.	.281E-05	.188E-01	.321E-03
1600.	.353E-05	.222E-01	-.448E-03
1600.	.445E-05	.263E-01	-.1[illegible]2E-02
1600.	.560E-05	.313E-01	-.26[illegible]E-02
1600.	.705E-05	.374E-01	-.39[illegible]E-02
1600.	.887E-05	.450E-01	-.533E-02
1600.	.112E-04	.541E-01	-.656E-02
1600.	.141E-04	.652E-01	-.731E-02
1600.	.177E-04	.781E-01	-.726E-02
1600.	.223E-04	.925E-01	-.648E-02
1600.	.250E-04	.100E+00	-.604E-02
1600.	.281E-04	.109E+00	-.563E-02
1600.	.353E-04	.128E+00	-.468E-02
1600.	.445E-04	.152E+00	-.292E-02
1600.	.560E-04	.180E+00	.151E-03
1600.	.887E-04	.252E+00	.119E-01
1800.	.177E-05	.147E-01	.941E-03
1800.	.281E-05	.205E-01	-.308E-03
1800.	.353E-05	.243E-01	-.121E-02
1800.	.445E-05	.289E-01	-.231E-02
1800.	.560E-05	.345E-01	-.359E-02
1800.	.705E-05	.414E-01	-.494E-02
1800.	.887E-05	.498E-01	-.618E-02
1800.	.112E-04	.600E-01	-.704E-02
1800.	.141E-04	.719E-01	-.719E-02
1800.	.177E-04	.854E-01	-.662E-02
1800.	.223E-04	.101E+00	-.591E-02
1800.	.250E-04	.109E+00	-.560E-02
1800.	.281E-04	.118E+00	-.522E-02
1800.	.353E-04	.140E+00	-.393E-02
1800.	.445E-04	.166E+00	-.153E-02
1800.	.560E-04	.196E+00	.235E-02
2000.	.223E-05	.188E-01	-.116E-03

MACH NO. = 1.0 BETA = .01
TWALL =300.00 TSTAR =250.00

R	FR	AR	AI
2000.	.281E-05	.222E-01	-.934E-03
2000.	.353E-05	.264E-01	-.195E-02
2000.	.445E-05	.315E-01	-.315E-02
2000.	.560E-05	.378E-01	-.445E-02
2000.	.705E-05	.454E-01	-.571E-02
2000.	.887E-05	.547E-01	-.669E-02
2000.	.112E-04	.656E-01	-.708E-02
2000.	.141E-04	.781E-01	-.674E-02
2000.	.177E-04	.920E-01	-.613E-02
2000.	.223E-04	.108E+00	-.563E-02
2000.	.250E-04	.118E+00	-.528E-02
2000.	.281E-04	.128E+00	-.476E-02
2000.	.353E-04	.151E+00	-.298E-02
2000.	.445E-04	.179E+00	.472E-04
2000.	.705E-04	.251E+00	.116E-01
2200.	.177E-05	.171E-01	.987E-04
2200.	.223E-05	.202E-01	-.631E-03
2200.	.281E-05	.240E-01	-.155E-02
2200.	.353E-05	.285E-01	-.266E-02
2200.	.445E-05	.341E-01	-.391E-02
2200.	.560E-05	.410E-01	-.517E-02
2200.	.705E-05	.494E-01	-.625E-02
2200.	.887E-05	.594E-01	-.687E-02
2200.	.112E-04	.708E-01	-.680E-02
2200.	.141E-04	.836E-01	-.630E-02
2200.	.177E-04	.983E-01	-.590E-02
2200.	.223E-04	.116E+00	-.537E-02
2200.	.250E-04	.126E+00	-.488E-02
2200.	.281E-04	.137E+00	-.415E-02
2200.	.353E-04	.162E+00	-.189E-02
2200.	.560E-04	.227E+00	.729E-02
2400.	.141E-05	.154E-01	.317E-03
2400.	.177E-05	.182E-01	-.322E-03
2400.	.223E-05	.216E-01	-.114E-02
2400.	.281E-05	.257E-01	-.215E-02
2400.	.353E-05	.307E-01	-.332E-02
2400.	.445E-05	.368E-01	-.457E-02
2400.	.560E-05	.443E-01	-.572E-02
2400.	.705E-05	.533E-01	-.655E-02
2400.	.887E-05	.638E-01	-.678E-02
2400.	.112E-04	.756E-01	-.644E-02
2400.	.141E-04	.889E-01	-.606E-02
2400.	.177E-04	.105E+00	-.576E-02
2400.	.223E-04	.124E+00	-.502E-02
2400.	.250E-04	.134E+00	-.435E-02
2400.	.281E-04	.146E+00	-.343E-02
2400.	.353E-04	.173E+00	-.692E-03
2400.	.445E-04	.205E+00	.360E-02

MACH NO. = 1.0 BETA = -.1
TWALL =300.00 TSTAR =250.00

R	FR	AR	AI
2600.	.141E-05	.164E-01	-.263E-04
2600.	.177E-05	.134E-01	-.745E-03
2600.	.223E-05	.230E-01	-.165E-02
2600.	.281E-05	.274E-01	-.273E-02
2600.	.353E-05	.328E-01	-.392E-02
2600.	.445E-05	.395E-01	-.512E-02
2600.	.560E-05	.475E-01	-.611E-02
2600.	.705E-05	.570E-01	-.663E-02
2600.	.887E-05	.679E-01	-.654E-02
2600.	.112E-04	.800E-01	-.617E-02
2600.	.141E-04	.940E-01	-.596E-02
2600.	.177E-04	.111E+00	-.559E-02
2600.	.223E-04	.131E+00	-.457E-02
2600.	.250E-04	.142E+00	-.372E-02
2600.	.281E-04	.155E+00	-.261E-02
2600.	.445E-04	.217E+00	.556E-02

MACH NO. = 1.8 BETA = -.05
TWALL =300.00 TSTAR =250.00

R	FR	AR	AI
175.	.160E-03	.682E-01	.405E-02
250.	.500E-04	.376E-01	.580E-02
250.	.675E-04	.471E-01	.435E-02
250.	.849E-04	.560E-01	.301E-02
250.	.107E-03	.666E-01	.143E-02
250.	.135E-03	.803E-01	-.302E-03
250.	.151E-03	.878E-01	-.118E-02
250.	.160E-03	.919E-01	-.160E-02
250.	.169E-03	.963E-01	-.200E-02
250.	.190E-03	.106E+00	-.272E-02
250.	.213E-03	.117E+00	-.325E-02
250.	.239E-03	.125E+00	-.347E-02
250.	.269E-03	.141E+00	-.325E-02
275.	.160E-03	.130E+00	-.291E-02
325.	.160E-03	.116E+00	-.445E-02
350.	.500E-04	.490E-01	.199E-02
375.	.160E-03	.133E+00	-.436E-02
400.	.334E-04	.402E-01	.270E-02
400.	.421E-04	.478E-01	.146E-02
400.	.500E-04	.545E-01	.358E-03
400.	.530E-04	.570E-01	-.363E-04
400.	.594E-04	.623E-01	-.859E-03
400.	.667E-04	.683E-01	-.171E-02
400.	.748E-04	.748E-01	-.257E-02
400.	.750E-04	.750E-01	-.259E-02
400.	.794E-04	.786E-01	-.301E-02
400.	.891E-04	.863E-01	-.379E-02
400.	.100E-03	.949E-01	-.445E-02
400.	.112E-03	.104E+00	-.490E-02
400.	.126E-03	.115E+00	-.504E-02
400.	.141E-03	.127E+00	-.471E-02
400.	.159E-03	.139E+00	-.376E-02
400.	.160E-03	.140E+00	-.365E-02
400.	.169E-03	.147E+00	-.285E-02
400.	.190E-03	.152E+00	-.574E-03
400.	.213E-03	.176E+00	.262E-02
450.	.500E-04	.601E-01	-.114E-02
500.	.500E-04	.714E-01	-.364E-02
600.	.188E-04	.359E-01	.161E-02
600.	.237E-04	.427E-01	.406E-03
600.	.265E-04	.466E-01	-.284E-03
600.	.298E-04	.509E-01	-.103E-02
600.	.334E-04	.557E-01	-.182E-02
600.	.375E-04	.611E-01	-.264E-02
600.	.421E-04	.670E-01	-.346E-02
600.	.472E-04	.735E-01	-.423E-02
600.	.500E-04	.771E-01	-.458E-02
600.	.530E-04	.808E-01	-.491E-02

MACH NO. = 1.8 BETA = -.05
TWALL =300.00 TSTAR =250.00

R	FR	AR	AI
600.	.594E-04	.889E-01	-.542E-02
600.	.667E-04	.979E-01	-.568E-02
600.	.748E-04	.108E+00	-.556E-02
600.	.839E-04	.118E+00	-.494E-02
600.	.940E-04	.130E+00	-.371E-02
600.	.942E-04	.130E+00	-.369E-02
600.	.996E-04	.136E+00	-.282E-02
600.	.112E-03	.148E+00	-.526E-03
600.	.141E-03	.174E+00	.500E-02
600.	.177E-03	.204E+00	.996E-02
650.	.500E-04	.829E-01	-.528E-02
750.	.500E-04	.944E-01	-.584E-02
800.	.150E-04	.380E-01	.116E-03
800.	.168E-04	.415E-01	-.531E-03
800.	.212E-04	.496E-01	-.198E-02
800.	.267E-04	.596E-01	-.354E-02
800.	.336E-04	.720E-01	-.497E-02
800.	.423E-04	.871E-01	-.582E-02
800.	.500E-04	.100E+00	-.568E-02
800.	.532E-04	.105E+00	-.538E-02
800.	.670E-04	.126E+00	-.284E-02
1000.	.532E-05	.208E-01	.246E-02
1000.	.844E-05	.294E-01	.974E-03
1000.	.106E-04	.356E-01	-.835E-04
1000.	.134E-04	.416E-01	-.137E-02
1000.	.150E-04	.457E-01	-.209E-02
1000.	.168E-04	.500E-01	-.263E-02
1000.	.212E-04	.603E-01	-.431E-02
1000.	.267E-04	.728E-01	-.549E-02
1000.	.336E-04	.881E-01	-.586E-02
1000.	.423E-04	.106E+00	-.466E-02
1000.	.532E-04	.126E+00	-.158E-02
1000.	.670E-04	.147E+00	.186E-02
1200.	.532E-05	.241E-01	.143E-02
1200.	.844E-05	.340E-01	-.469E-03
1200.	.106E-04	.406E-01	-.175E-02
1200.	.134E-04	.488E-01	-.318E-02
1200.	.150E-04	.535E-01	-.389E-02
1200.	.168E-04	.586E-01	-.457E-02
1200.	.212E-04	.710E-01	-.560E-02
1200.	.267E-04	.858E-01	-.573E-02
1200.	.336E-04	.103E+00	-.429E-02
1200.	.423E-04	.122E+00	-.136E-02
1200.	.670E-04	.167E+00	.406E-02
1400.	.423E-05	.229E-01	.126E-02
1400.	.670E-05	.324E-01	-.586E-03
1400.	.844E-05	.387E-01	-.183E-02
1400.	.106E-04	.464E-01	-.321E-02

MACH NO. = 1.0 BETA = -.05
TWALL =300.00 TSTAR =250.00

R	FR	AR	AI
1400.	.134E-04	.559E-01	-.455E-02
1400.	.150E-04	.615E-01	-.512E-02
1400.	.168E-04	.676E-01	-.554E-02
1400.	.212E-04	.816E-01	-.566E-02
1400.	.267E-04	.978E-01	-.429E-02
1400.	.336E-04	.115E+00	-.167E-02
1400.	.532E-04	.158E+00	.294E-02
1600.	.336E-05	.214E-01	.122E-02
1600.	.532E-05	.303E-01	-.525E-03
1600.	.670E-05	.361E-01	-.171E-02
1600.	.844E-05	.433E-01	-.304E-02
1600.	.106E-04	.522E-01	-.436E-02
1600.	.134E-04	.631E-01	-.538E-02
1600.	.150E-04	.694E-01	-.564E-02
1600.	.150E-04	.694E-01	-.564E-02
1600.	.168E-04	.762E-01	-.563E-02
1600.	.212E-04	.913E-01	-.453E-02
1600.	.267E-04	.108E+00	-.222E-02
1600.	.336E-04	.126E+00	-.168E-03
1600.	.532E-04	.174E+00	.488E-02
1600.	.670E-04	.206E+00	.966E-02
1800.	.267E-05	.198E-01	.126E-02
1800.	.423E-05	.279E-01	-.349E-03
1800.	.532E-05	.333E-01	-.146E-02
1800.	.670E-05	.400E-01	-.273E-02
1800.	.844E-05	.481E-01	-.404E-02
1800.	.106E-04	.581E-01	-.512E-02
1800.	.134E-04	.702E-01	-.558E-02
1800.	.150E-04	.770E-01	-.540E-02
1800.	.168E-04	.842E-01	-.486E-02
1800.	.212E-04	.997E-01	-.287E-02
1800.	.267E-04	.116E+00	-.934E-03
1800.	.336E-04	.137E+00	.678E-03
2000.	.212E-05	.181E-01	.134E-02
2000.	.336E-05	.256E-01	-.104E-03
2000.	.423E-05	.305E-01	-.113E-02
2000.	.532E-05	.365E-01	-.233E-02
2000.	.670E-05	.438E-01	-.361E-02
2000.	.844E-05	.529E-01	-.477E-02
2000.	.106E-04	.639E-01	-.545E-02
2000.	.134E-04	.769E-01	-.516E-02
2000.	.150E-04	.840E-01	-.451E-02
2000.	.168E-04	.914E-01	-.357E-02
2000.	.212E-04	.107E+00	-.167E-02
2000.	.267E-04	.125E+00	-.273E-03
2000.	.423E-04	.174E+00	.484E-02
2200.	.267E-05	.232E-01	.173E-03
2200.	.336E-05	.276E-01	-.757E-03

MACH NO. = 1.0 BETA = -.05
TWALL =300.00 TSTAR =250.00

R	FR	AR	AI
2200.	.423E-05	.330E-01	-.188E-02
2200.	.532E-05	.396E-01	-.311E-02
2200.	.670E-05	.477E-01	-.432E-02
2200.	.844E-05	.577E-01	-.520E-02
2200.	.106E-04	.695E-01	-.533E-02
2200.	.134E-04	.830E-01	-.425E-02
2200.	.150E-04	.902E-01	-.333E-02
2200.	.168E-04	.975E-01	-.242E-02
2200.	.212E-04	.114E+00	-.106E-02
2200.	.336E-04	.158E+00	.282E-02
2400.	.212E-05	.209E-01	.458E-03
2400.	.267E-05	.249E-01	-.368E-03
2400.	.336E-05	.297E-01	-.139E-02
2400.	.423E-05	.356E-01	-.257E-02
2400.	.532E-05	.428E-01	-.378E-02
2400.	.670E-05	.517E-01	-.482E-02
2400.	.844E-05	.624E-01	-.532E-02
2400.	.106E-04	.748E-01	-.480E-02
2400.	.134E-04	.884E-01	-.321E-02
2400.	.150E-04	.956E-01	-.239E-02
2400.	.168E-04	.103E+00	-.175E-02
2400.	.212E-04	.121E+00	-.635E-03
2400.	.267E-04	.142E+00	.115E-02
2400.	.423E-04	.198E+00	.845E-02
2600.	.267E-05	.266E-01	-.902E-03
2600.	.336E-05	.318E-01	-.193E-02
2600.	.423E-05	.381E-01	-.318E-02
2600.	.532E-05	.460E-01	-.432E-02
2600.	.670E-05	.555E-01	-.510E-02
2600.	.844E-05	.669E-01	-.512E-02
2600.	.106E-04	.796E-01	-.400E-02
2600.	.134E-04	.933E-01	-.243E-02
2600.	.150E-04	.101E+00	-.186E-02
2600.	.168E-04	.109E+00	-.139E-02
2600.	.212E-04	.128E+00	-.141E-03
2600.	.336E-04	.178E+00	.547E-02
2800.	.134E-05	.167E-01	.983E-03
2800.	.212E-05	.237E-01	-.432E-03
2800.	.267E-05	.283E-01	-.142E-02
2800.	.336E-05	.339E-01	-.255E-02
2800.	.423E-05	.408E-01	-.372E-02
2800.	.532E-05	.492E-01	-.470E-02
2800.	.670E-05	.593E-01	-.516E-02
2800.	.844E-05	.711E-01	-.464E-02
2800.	.106E-04	.839E-01	-.320E-02
2800.	.134E-04	.979E-01	-.193E-02
2800.	.150E-04	.106E+00	-.156E-02
2800.	.168E-04	.115E+00	-.108E-02

MACH NO. = 1.0 BETA = .10
TWALL =300.00 TSTAR =250.00

R	FR	AR	AI
500.	.564E-04	.720E-01	.313E-02
500.	.632E-04	.791E-01	.244E-02
500.	.100E-03	.116E+00	.610E-03
500.	.159E-03	.173E+00	.613E-02
500.	.224E-03	.224E+00	.260E-01
600.	.564E-04	.849E-01	.970E-03
600.	.796E-04	.114E+00	-.275E-04
600.	.126E-03	.168E+00	.640E-02
700.	.564E-04	.981E-01	-.393E-03
700.	.632E-04	.108E+00	-.502E-03
700.	.796E-04	.132E+00	.724E-03
700.	.126E-03	.191E+00	.169E-01
800.	.200E-04	.474E-01	.357E-02
800.	.224E-04	.520E-01	.299E-02
800.	.283E-04	.625E-01	.171E-02
800.	.448E-04	.916E-01	-.645E-03
800.	.564E-04	.111E+00	-.705E-03
800.	.710E-04	.136E+00	.145E-02
800.	.100E-03	.179E+00	.140E-01
850.	.564E-04	.118E+00	-.387E-03
1000.	.200E-04	.577E-01	.130E-02
1000.	.283E-04	.767E-01	-.603E-03
1000.	.356E-04	.932E-01	-.133E-02
1000.	.448E-04	.113E+00	-.695E-03
1000.	.710E-04	.169E+00	.118E-01
1000.	.112E-03	.216E+00	.259E-01
1000.	.142E-03	.254E+00	.331E-01
1200.	.142E-04	.513E-01	.136E-02
1200.	.200E-04	.681E-01	-.550E-03
1200.	.224E-04	.750E-01	-.110E-02
1200.	.283E-04	.912E-01	-.166E-02
1200.	.356E-04	.111E+00	-.728E-03
1200.	.448E-04	.135E+00	.348E-02
1200.	.710E-04	.180E+00	.202E-01
1400.	.112E-04	.489E-01	.111E-02
1400.	.142E-04	.590E-01	-.159E-03
1400.	.178E-04	.714E-01	-.131E-02
1400.	.200E-04	.787E-01	-.171E-02
1400.	.224E-04	.869E-01	-.188E-02
1400.	.283E-04	.106E+00	-.991E-03
1400.	.356E-04	.128E+00	.297E-02
1400.	.564E-04	.171E+00	.184E-01
1600.	.893E-05	.458E-01	.107E-02
1600.	.112E-04	.552E-01	-.169E-03
1600.	.142E-04	.668E-01	-.134E-02
1600.	.178E-04	.811E-01	-.202E-02
1600.	.200E-04	.895E-01	-.195E-02
1600.	.224E-04	.988E-01	-.143E-02

MACH NO. = 1.0 BETA = .10
TWALL =300.00 TSTAR =250.00

R	FR	AR	AI
1600.	.283E-04	.120E+00	.188E-02
1600.	.448E-04	.160E+00	.165E-01
1638.	.700E-05	.383E-01	.208E-02
1630.	.700E-05	.383E-01	.208E-02
1630.	.989E-05	.505E-01	.357E-03
1630.	.124E-04	.610E-01	-.276E-03
1630.	.157E-04	.740E-01	-.184E-02
1630.	.197E-04	.901E-01	-.194E-02
1630.	.248E-04	.110E+00	-.697E-04
1630.	.394E-04	.151E+00	.145E-01
1730.	.700E-05	.403E-01	.158E-02
1800.	.785E-05	.458E-01	.665E-03
1800.	.989E-05	.553E-01	-.561E-03
1800.	.124E-04	.670E-01	-.166E-02
1800.	.157E-04	.814E-01	-.216E-02
1800.	.197E-04	.991E-01	-.119E-02
1800.	.313E-04	.140E+00	.112E-01
1930.	.700E-05	.444E-01	.634E-03
2000.	.624E-05	.418E-01	.902E-03
2000.	.785E-05	.504E-01	-.269E-03
2000.	.989E-05	.610E-01	-.144E-02
2000.	.124E-04	.741E-01	-.219E-02
2000.	.157E-04	.901E-01	-.183E-02
2000.	.197E-04	.109E+00	.925E-03
2000.	.313E-04	.147E+00	.141E-01
2130.	.700E-05	.486E-01	-.243E-03
2200.	.394E-05	.315E-01	.215E-02
2200.	.624E-05	.455E-01	.718E-04
2200.	.700E-05	.500E-01	-.526E-03
2200.	.700E-05	.500E-01	-.526E-03
2200.	.785E-05	.550E-01	-.111E-02
2200.	.989E-05	.667E-01	-.206E-02
2200.	.124E-04	.812E-01	-.224E-02
2200.	.157E-04	.987E-01	-.633E-03
2200.	.248E-04	.136E+00	.120E-01
2230.	.700E-05	.506E-01	-.643E-03
2330.	.700E-05	.527E-01	-.101E-02
2400.	.248E-05	.236E-01	.301E-02
2400.	.394E-05	.340E-01	.153E-02
2400.	.624E-05	.493E-01	-.660E-03
2400.	.700E-05	.542E-01	-.125E-02
2400.	.785E-05	.597E-01	-.176E-02
2400.	.989E-05	.726E-01	-.236E-02
2400.	.124E-04	.883E-01	-.171E-02
2400.	.197E-04	.125E+00	.678E-02
2400.	.313E-04	.165E+00	.156E-01
2430.	.700E-05	.543E-01	-.135E-02
2400.	.700E-05	.559E-01	-.151E-02

MACH NO. = 1.0 BETA = .10
TWALL =300.00 TSTAR =250.00

R	FR	AR	AI
2480.	.700E-05	.559E-01	-.158E-02
2480.	.700E-05	.559E-01	-.158E-02
2480.	.700E-05	.559E-01	-.158E-02
2480.	.700E-05	.559E-01	-.158E-02
2520.	.700E-05	.588E-01	-.178E-02
2520.	.700E-05	.588E-01	-.178E-02
2680.	.700E-05	.602E-01	-.202E-02
2680.	.700E-05	.602E-01	-.202E-02
2760.	.700E-05	.623E-01	-.221E-02
2760.	.700E-05	.623E-01	-.221E-02
2800.	.157E-05	.187E-01	.324E-02
2840.	.248E-05	.278E-01	.217E-02
2880.	.394E-05	.390E-01	.334E-03
2920.	.496E-05	.470E-01	-.802E-03
2960.	.624E-05	.569E-01	-.186E-02
2960.	.700E-05	.627E-01	-.224E-02
2960.	.785E-05	.692E-01	-.243E-02
2960.	.989E-05	.842E-01	-.180E-02
2960.	.124E-04	.102E+00	.137E-02
2880.	.700E-05	.645E-01	-.235E-02
2880.	.700E-05	.645E-01	-.235E-02
2980.	.700E-05	.666E-01	-.244E-02
2980.	.700E-05	.666E-01	-.244E-02
3080.	.700E-05	.688E-01	-.248E-02
3080.	.700E-05	.688E-01	-.246E-02
3160.	.700E-05	.709E-01	-.246E-02
3160.	.700E-05	.709E-01	-.246E-02
3280.	.700E-05	.731E-01	-.238E-02
3280.	.700E-05	.731E-01	-.238E-02
3330.	.700E-05	.742E-01	-.231E-02
3330.	.700E-05	.742E-01	-.231E-02
3330.	.700E-05	.742E-01	-.231E-02
3330.	.700E-05	.742E-01	-.231E-02
3330.	.700E-05	.742E-01	-.231E-02
3330.	.700E-05	.742E-01	-.231E-02
3330.	.700E-05	.742E-01	-.231E-02
3330.	.700E-05	.742E-01	-.231E-02
3330.	.700E-05	.742E-01	-.231E-02
3330.	.700E-05	.742E-01	-.231E-02
3330.	.700E-05	.742E-01	-.231E-02

MACH NO. = 1.0 BETA = .2
TWALL =308.00 TSTAR =250.00

R	FR	AR	AI
1400.	.100E-04	.446E-01	.396E-02
1420.	.141E-04	.598E-01	.230E-02
1440.	.224E-04	.869E-01	.252E-03
1460.	.244E-04	.936E-01	.135E-03
1480.	.274E-04	.103E+00	.285E-03
1500.	.290E-04	.109E+00	.540E-03
1400.	.325E-04	.120E+00	.155E-02
1400.	.447E-04	.157E+00	.105E-01
1450.	.100E-04	.460E-01	.366E-02
1500.	.112E-04	.521E-01	.280E-02
1510.	.178E-04	.763E-01	.516E-03
1520.	.224E-04	.930E-01	-.226E-04
1500.	.282E-04	.114E+00	.910E-03
1520.	.447E-04	.167E+00	.166E-01
1540.	.100E-04	.503E-01	.276E-02
1560.	.140E-04	.663E-01	.104E-02
1580.	.148E-04	.696E-01	.761E-03
1600.	.178E-04	.812E-01	.530E-04
1600.	.187E-04	.847E-01	-.652E-04
1620.	.209E-04	.935E-01	-.150E-03
1600.	.224E-04	.991E-01	-.338E-04
1600.	.235E-04	.103E+00	.154E-03
1610.	.282E-04	.121E+00	.192E-02
1660.	.355E-04	.147E+00	.836E-02
1650.	.100E-04	.517E-01	.247E-02
1700.	.141E-04	.708E-01	.457E-03
1720.	.178E-04	.862E-01	-.250E-03
1780.	.200E-04	.952E-01	-.221E-03
1700.	.224E-04	.105E+00	.254E-03
1720.	.282E-04	.128E+00	.351E-02
1760.	.355E-04	.155E+00	.128E-01
1800.	.133E-04	.712E-01	.235E-03
1800.	.141E-04	.748E-01	.104E-04
1800.	.158E-04	.825E-01	-.311E-03
1800.	.178E-04	.911E-01	-.375E-03
1820.	.200E-04	.101E+00	-.445E-04
1800.	.224E-04	.111E+00	.877E-03
1800.	.282E-04	.138E+00	.575E-02
1850.	.355E-04	.161E+00	.186E-01
1900.	.100E-04	.589E-01	.113E-02
1920.	.126E-04	.714E-01	.474E-04
1960.	.133E-04	.750E-01	-.163E-03
1900.	.133E-04	.750E-01	-.163E-03
1920.	.141E-04	.788E-01	-.338E-03
1900.	.158E-04	.870E-01	-.488E-03
1900.	.178E-04	.961E-01	-.301E-03
1900.	.200E-04	.106E+00	.404E-03
1950.	.251E-04	.130E+00	.448E-02

MACH NO. = 1.0 BETA = .2
TWALL =308.00 TSTAR =250.00

R	FR	AR	AI
2000.	.794E-05	.511E-01	.182E-02
2020.	.100E-04	.612E-01	.656E-03
2000.	.126E-04	.751E-01	-.308E-03
2040.	.133E-04	.786E-01	-.460E-03
2060.	.133E-04	.788E-01	-.460E-03
2080.	.141E-04	.828E-01	-.553E-03
2100.	.158E-04	.915E-01	-.505E-03
2060.	.178E-04	.101E+00	-.811E-05
2000.	.200E-04	.112E+00	.115E-02
2080.	.251E-04	.139E+00	.690E-02
2050.	.100E-04	.632E-01	.436E-03
2100.	.708E-05	.486E-01	.195E-02
2120.	.891E-05	.580E-01	.786E-03
2100.	.112E-04	.713E-01	-.244E-03
2160.	.126E-04	.787E-01	-.569E-03
2180.	.133E-04	.827E-01	-.646E-03
2100.	.133E-04	.827E-01	-.646E-03
2100.	.141E-04	.869E-01	-.647E-03
2140.	.158E-04	.961E-01	-.345E-03
2160.	.178E-04	.108E+00	.528E-03
2180.	.224E-04	.129E+00	.520E-02
2160.	.282E-04	.153E+00	.176E-01
2220.	.891E-05	.614E-01	.372E-03
2220.	.944E-05	.644E-01	.106E-03
2220.	.100E-04	.676E-01	-.140E-03
2220.	.100E-04	.676E-01	-.140E-03
2220.	.106E-04	.710E-01	-.356E-03
2200.	.112E-04	.746E-01	-.534E-03
2220.	.119E-04	.784E-01	-.662E-03
2240.	.133E-04	.866E-01	-.712E-03
2200.	.133E-04	.866E-01	-.711E-03
2220.	.141E-04	.910E-01	-.599E-03
2200.	.150E-04	.957E-01	-.368E-03
2220.	.168E-04	.108E+00	.564E-03
2220.	.188E-04	.117E+00	.236E-02
2200.	.224E-04	.135E+00	.767E-02
2280.	.251E-04	.147E+00	.140E-01
2250.	.133E-04	.885E-01	-.695E-03
2300.	.688E-05	.516E-01	.126E-02
2320.	.866E-05	.625E-01	.131E-03
2340.	.917E-05	.656E-01	-.122E-03
2360.	.917E-05	.656E-01	-.122E-03
2380.	.972E-05	.689E-01	-.349E-03
2400.	.103E-04	.724E-01	-.542E-03
2420.	.109E-04	.760E-01	-.689E-03
2440.	.115E-04	.799E-01	-.778E-03
2460.	.122E-04	.840E-01	-.794E-03
2480.	.130E-04	.882E-01	-.721E-03

MACH NO. = 1.0 BETA = .2
TWALL =300.00 TSTAR =258.80

R	FR	AR	AI
2300.	.133E-04	.985E-01	-.645E-03
2300.	.133E-04	.985E-01	-.645E-03
2300.	.137E-04	.928E-01	-.538E-03
2300.	.145E-04	.975E-01	-.221E-03
2400.	.501E-05	.415E-01	.248E-02
2400.	.631E-05	.580E-01	.131E-02
2400.	.794E-05	.685E-01	.175E-03
2400.	.891E-05	.667E-01	-.323E-03
2400.	.100E-04	.736E-01	-.696E-03
2400.	.112E-04	.813E-01	-.859E-03
2400.	.126E-04	.898E-01	-.692E-03
2400.	.133E-04	.944E-01	-.436E-03
2400.	.133E-04	.944E-01	-.436E-03
2400.	.141E-04	.992E-01	-.284E-04
2400.	.158E-04	.110E+00	.137E-02
2500.	.562E-05	.472E-01	.152E-02
2500.	.708E-05	.571E-01	.375E-03
2500.	.794E-05	.629E-01	-.156E-03
2500.	.891E-05	.694E-01	-.596E-03
2500.	.100E-04	.766E-01	-.871E-03
2500.	.112E-04	.846E-01	-.880E-03
2500.	.126E-04	.935E-01	-.482E-03
2500.	.133E-04	.983E-01	-.706E-04
2500.	.133E-04	.983E-01	-.706E-04
2500.	.141E-04	.103E+00	.524E-03
2600.	.501E-05	.446E-01	.173E-02
2600.	.631E-05	.538E-01	.598E-03
2600.	.794E-05	.653E-01	-.446E-03
2600.	.891E-05	.721E-01	-.813E-03
2600.	.100E-04	.796E-01	-.969E-03
2600.	.112E-04	.880E-01	-.797E-03
2600.	.126E-04	.972E-01	-.128E-03
2700.	.398E-05	.383E-01	.244E-02
2700.	.501E-05	.461E-01	.140E-02
2700.	.631E-05	.558E-01	.272E-03
2700.	.708E-05	.614E-01	-.255E-03
2700.	.794E-05	.678E-01	-.693E-03
2700.	.891E-05	.748E-01	-.978E-03
2700.	.100E-04	.826E-01	-.985E-03
2700.	.112E-04	.913E-01	-.601E-03
2700.	.126E-04	.101E+00	.361E-03
2700.	.133E-04	.106E+00	.118E-02

MACH NO. = 1.0 BETA = .5
TWALL =300.00 TSTAR =250.00

R	FR	AR	AI
1300.	.600E-05	.253E-01	.180E-01
1400.	.600E-05	.278E-01	.964E-02
1500.	.600E-05	.301E-01	.927E-02
1600.	.600E-05	.323E-01	.891E-02
1700.	.600E-05	.345E-01	.855E-02
1800.	.600E-05	.366E-01	.821E-02
1900.	.600E-05	.386E-01	.786E-02
2000.	.600E-05	.406E-01	.752E-02
2100.	.600E-05	.426E-01	.718E-02
2200.	.184E-05	.136E-01	.800E-02
2200.	.291E-05	.233E-01	.883E-02
2200.	.461E-05	.357E-01	.747E-02
2200.	.600E-05	.446E-01	.684E-02
2200.	.920E-05	.636E-01	.518E-02
2200.	.130E-04	.851E-01	.361E-02
2200.	.130E-04	.851E-01	.361E-02
2200.	.184E-04	.115E+00	.328E-02
2200.	.291E-04	.175E+00	.125E-01
2200.	.461E-04	.284E+00	.809E-01
2200.	.731E-04	.561E+00	.210E+00
2225.	.130E-04	.861E-01	.351E-02
2300.	.600E-05	.465E-01	.649E-02
2375.	.130E-04	.918E-01	.299E-02
2425.	.130E-04	.939E-01	.285E-02
2500.	.600E-05	.503E-01	.580E-02
2550.	.600E-05	.512E-01	.563E-02
2600.	.184E-05	.179E-01	.757E-02
2600.	.291E-05	.282E-01	.728E-02
2600.	.461E-05	.419E-01	.636E-02
2600.	.600E-05	.521E-01	.546E-02
2600.	.920E-05	.746E-01	.350E-02
2600.	.130E-04	.101E+00	.251E-02
2600.	.184E-04	.137E+00	.497E-02
2600.	.291E-04	.209E+00	.320E-01
2600.	.461E-04	.394E+00	.135E+00
2600.	.731E-04	.768E+00	.307E+00
2650.	.600E-05	.531E-01	.528E-02
2850.	.600E-05	.568E-01	.461E-02
3050.	.600E-05	.606E-01	.395E-02
3250.	.600E-05	.644E-01	.333E-02
3450.	.600E-05	.682E-01	.276E-02
3500.	.600E-05	.692E-01	.262E-02
3700.	.600E-05	.730E-01	.212E-02
3900.	.600E-05	.769E-01	.170E-02
4100.	.600E-05	.809E-01	.135E-02
4300.	.600E-05	.849E-01	.110E-02
4400.	.600E-05	.869E-01	.102E-02
4475.	.600E-05	.884E-01	.970E-03

MACH NO. = 1.0 BETA = .5
TWALL =300.00 TSTAR =250.00

R	FR	AR	AI
4525.	.600E-05	.894E-01	.946E-03
4600.	.848E-06	.167E-01	.603E-02
4600.	.134E-05	.257E-01	.567E-02
4600.	.213E-05	.378E-01	.466E-02
4600.	.337E-05	.554E-01	.279E-02
4600.	.535E-05	.821E-01	.972E-03
4600.	.600E-05	.909E-01	.925E-03
4600.	.848E-05	.124E+00	.403E-02
4600.	.134E-04	.189E+00	.388E-01
4625.	.600E-05	.914E-01	.922E-03
4675.	.600E-05	.925E-01	.920E-03
4700.	.600E-05	.930E-01	.922E-03
4800.	.268E-05	.476E-01	.346E-02
4900.	.268E-05	.485E-01	.328E-02
5000.	.268E-05	.494E-01	.311E-02
5100.	.268E-05	.504E-01	.293E-02
5200.	.268E-05	.513E-01	.276E-02
5300.	.268E-05	.523E-01	.259E-02
5400.	.268E-05	.532E-01	.242E-02
5600.	.268E-05	.551E-01	.209E-02
5800.	.268E-05	.570E-01	.178E-02
6000.	.268E-05	.589E-01	.148E-02
6100.	.268E-05	.583E-01	.148E-02
6300.	.260E-05	.602E-01	.121E-02
6500.	.260E-05	.620E-01	.952E-03
6700.	.260E-05	.639E-01	.719E-03
6900.	.260E-05	.658E-01	.509E-03
7000.	.260E-05	.668E-01	.414E-03
7000.	.275E-05	.702E-01	.246E-03
7000.	.309E-05	.777E-01	.623E-04
7000.	.367E-05	.906E-01	.401E-03
7000.	.436E-05	.106E+00	.204E-02
7000.	.490E-05	.118E+00	.437E-02
7000.	.582E-05	.137E+00	.113E-01
7000.	.692E-05	.160E+00	.281E-01
7000.	.822E-05	.206E+00	.599E-01
7200.	.260E-05	.687E-01	.241E-03
7300.	.263E-05	.704E-01	.138E-03
7300.	.275E-05	.733E-01	.473E-04
7300.	.288E-05	.763E-01	-.468E-05
7500.	.260E-05	.716E-01	.339E-04
7500.	.263E-05	.723E-01	.133E-04
7500.	.269E-05	.738E-01	-.208E-04
7500.	.275E-05	.753E-01	-.447E-04
7500.	.282E-05	.769E-01	-.575E-04
7500.	.288E-05	.785E-01	-.581E-04
7500.	.347E-05	.925E-01	.529E-03
7500.	.436E-05	.114E+00	.384E-02

MACH NO. = 1.0 BETA = .5
TWALL =300.00 TSTAR =250.00

R	FR	AR	AI
7500.	.550E-05	.148E+00	.138E-01
7510.	.692E-05	.183E+00	.477E-01
7600.	.238E-05	.673E-01	.173E-03
7610.	.260E-05	.726E-01	-.209E-04
7620.	.260E-05	.726E-01	-.289E-04
7630.	.268E-05	.744E-01	-.578E-04
7700.	.283E-05	.783E-01	-.793E-04
7710.	.300E-05	.825E-01	-.169E-04
7720.	.260E-05	.736E-01	-.683E-04
7800.	.159E-05	.489E-01	.163E-02
7810.	.179E-05	.539E-01	.110E-02
7820.	.201E-05	.595E-01	.606E-03
7830.	.225E-05	.657E-01	.189E-03
7840.	.253E-05	.727E-01	-.761E-04
7850.	.260E-05	.745E-01	-.108E-03
7860.	.260E-05	.745E-01	-.108E-03
7870.	.268E-05	.765E-01	-.122E-03
7880.	.283E-05	.805E-01	-.913E-04
7890.	.318E-05	.892E-01	.282E-03
7900.	.357E-05	.989E-01	.124E-02
7910.	.400E-05	.110E+00	.309E-02
7950.	.260E-05	.750E-01	-.125E-03
8000.	.260E-05	.755E-01	-.140E-03
8010.	.213E-05	.641E-01	.214E-03
8020.	.238E-05	.709E-01	-.837E-04
8030.	.253E-05	.746E-01	-.154E-03
8080.	.260E-05	.765E-01	-.163E-03
8090.	.260E-05	.765E-01	-.163E-03
8100.	.268E-05	.785E-01	-.153E-03
8110.	.283E-05	.826E-01	-.630E-04
8120.	.300E-05	.870E-01	.136E-03
8130.	.337E-05	.965E-01	.970E-03
8190.	.260E-05	.775E-01	-.179E-03
8200.	.201E-05	.625E-01	.249E-03
8210.	.225E-05	.691E-01	-.805E-04
8220.	.238E-05	.727E-01	-.174E-03
8230.	.253E-05	.765E-01	-.281E-03
8240.	.260E-05	.785E-01	-.146E-03
8290.	.260E-05	.785E-01	-.186E-03
8300.	.268E-05	.805E-01	-.147E-03
8310.	.283E-05	.847E-01	.756E-05
8320.	.318E-05	.940E-01	.718E-03
8360.	.260E-05	.795E-01	-.184E-03
8400.	.189E-05	.609E-01	.292E-03
8410.	.201E-05	.648E-01	.946E-04
8420.	.213E-05	.673E-01	-.666E-04
8460.	.225E-05	.708E-01	-.181E-03
8490.	.238E-05	.745E-01	-.236E-03

MACH NO. = 1.0 BETA = .5
TWALL =300.00 TSTAR =250.00

R	FR	AR	AI
8500.	.253E-05	.784E-01	-.216E-03
8510.	.260E-05	.804E-01	-.173E-03
8600.	.260E-05	.804E-01	-.173E-03
8610.	.268E-05	.825E-01	-.104E-03
8620.	.283E-05	.869E-01	.123E-03
8630.	.318E-05	.964E-01	.103E-02
8700.	.260E-05	.814E-01	-.153E-03
8710.	.179E-05	.593E-01	.343E-03
8720.	.201E-05	.656E-01	-.420E-04
8730.	.213E-05	.689E-01	-.177E-03
8740.	.225E-05	.725E-01	-.257E-03
8750.	.238E-05	.763E-01	-.270E-03
8760.	.253E-05	.803E-01	-.198E-03
8770.	.260E-05	.824E-01	-.124E-03
8780.	.260E-05	.824E-01	-.124E-03
8790.	.268E-05	.846E-01	-.209E-04
8800.	.283E-05	.891E-01	.285E-03
8810.	.318E-05	.988E-01	.141E-02
8870.	.260E-05	.834E-01	-.850E-04
8880.	.260E-05	.834E-01	-.849E-04
8890.	.260E-05	.839E-01	-.619E-04
8900.	.179E-05	.607E-01	.183E-03
8910.	.189E-05	.638E-01	-.716E-05
8920.	.201E-05	.671E-01	-.160E-03
8930.	.213E-05	.706E-01	-.265E-03
8940.	.225E-05	.743E-01	-.308E-03
8990.	.238E-05	.782E-01	-.274E-03
9000.	.253E-05	.823E-01	-.144E-03
9010.	.260E-05	.844E-01	-.363E-04
9020.	.268E-05	.866E-01	.104E-03
9030.	.300E-05	.961E-01	.107E-02
9050.	.260E-05	.849E-01	-.813E-05
9060.	.179E-05	.621E-01	.377E-04
9070.	.189E-05	.653E-01	-.132E-03
9080.	.201E-05	.686E-01	-.259E-03
9090.	.213E-05	.722E-01	-.330E-03
9100.	.225E-05	.760E-01	-.331E-03
9110.	.238E-05	.880E-01	-.246E-03
9200.	.253E-05	.842E-01	-.528E-04
9250.	.260E-05	.869E-01	.130E-03
9260.	.179E-05	.635E-01	-.935E-04
9270.	.189E-05	.667E-01	-.240E-03
9280.	.201E-05	.702E-01	-.338E-03
9290.	.213E-05	.739E-01	-.372E-03
9300.	.225E-05	.778E-01	-.327E-03
9310.	.238E-05	.819E-01	-.185E-03
9360.	.253E-05	.862E-01	.770E-04
9370.	.260E-05	.890E-01	.311E-03

MACH NO. = 1.8 BETA = .5
TWALL =300.00 TSTAR =250.00

R	FR	AR	AI
9400.	.159E-05	.587E-01	.155E-03
9420.	.169E-05	.617E-01	-.441E-04
9440.	.179E-05	.649E-01	-.289E-03
9460.	.189E-05	.682E-01	-.331E-03
9480.	.201E-05	.718E-01	-.395E-03
9500.	.213E-05	.755E-01	-.389E-03
9520.	.225E-05	.795E-01	-.294E-03
9540.	.238E-05	.837E-01	-.903E-04
9560.	.253E-05	.882E-01	.240E-03
9580.	.268E-05	.930E-01	.537E-03
9600.	.159E-05	.599E-01	.154E-04
9620.	.169E-05	.630E-01	-.167E-03
9640.	.179E-05	.663E-01	-.318E-03
9660.	.189E-05	.697E-01	-.402E-03
9680.	.201E-05	.733E-01	-.431E-03
9700.	.213E-05	.772E-01	-.388E-03
9720.	.225E-05	.813E-01	-.230E-03
9740.	.253E-05	.901E-01	.461E-03

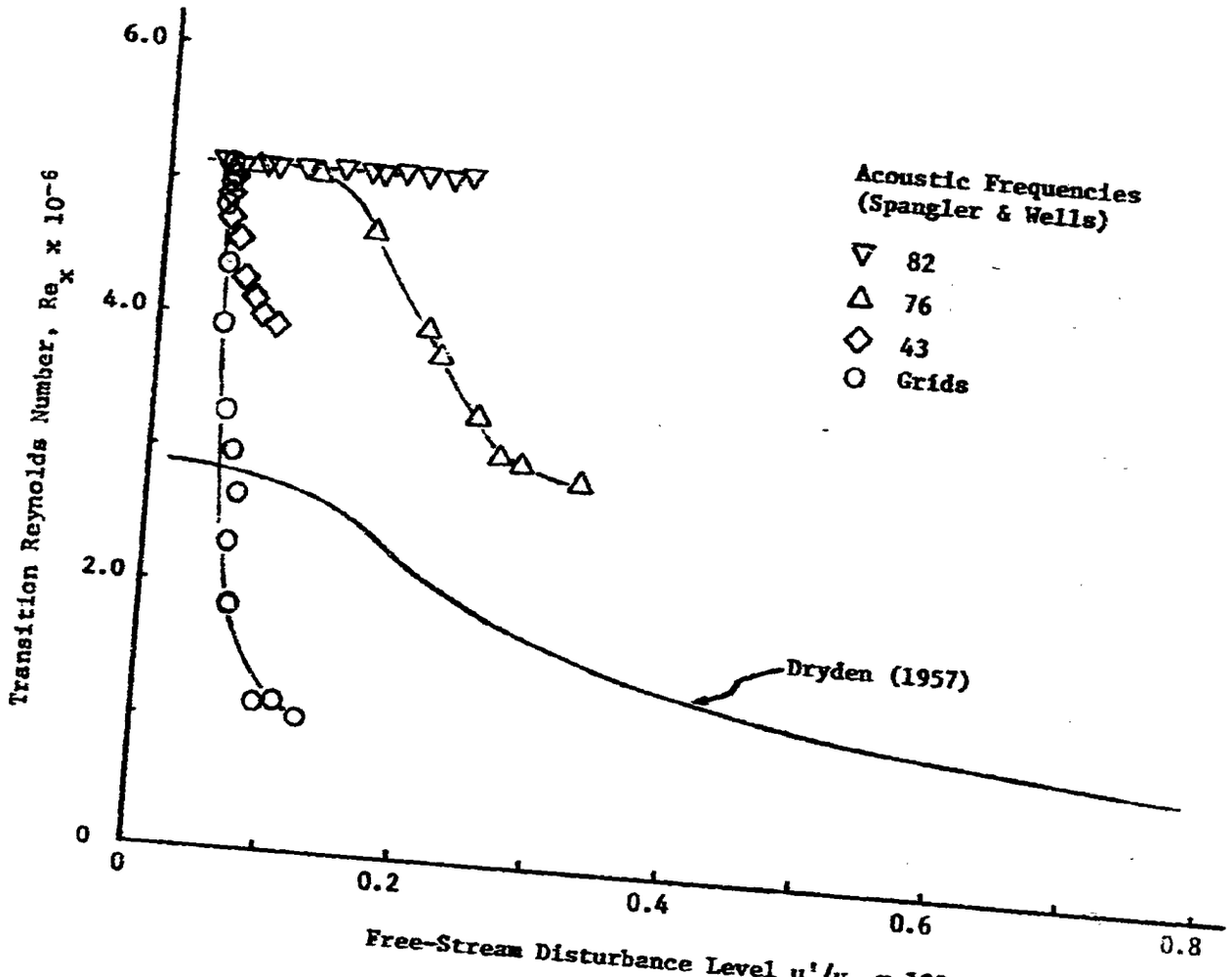

Fig. 1 Effect of Free-Stream Disturbances on Transition.

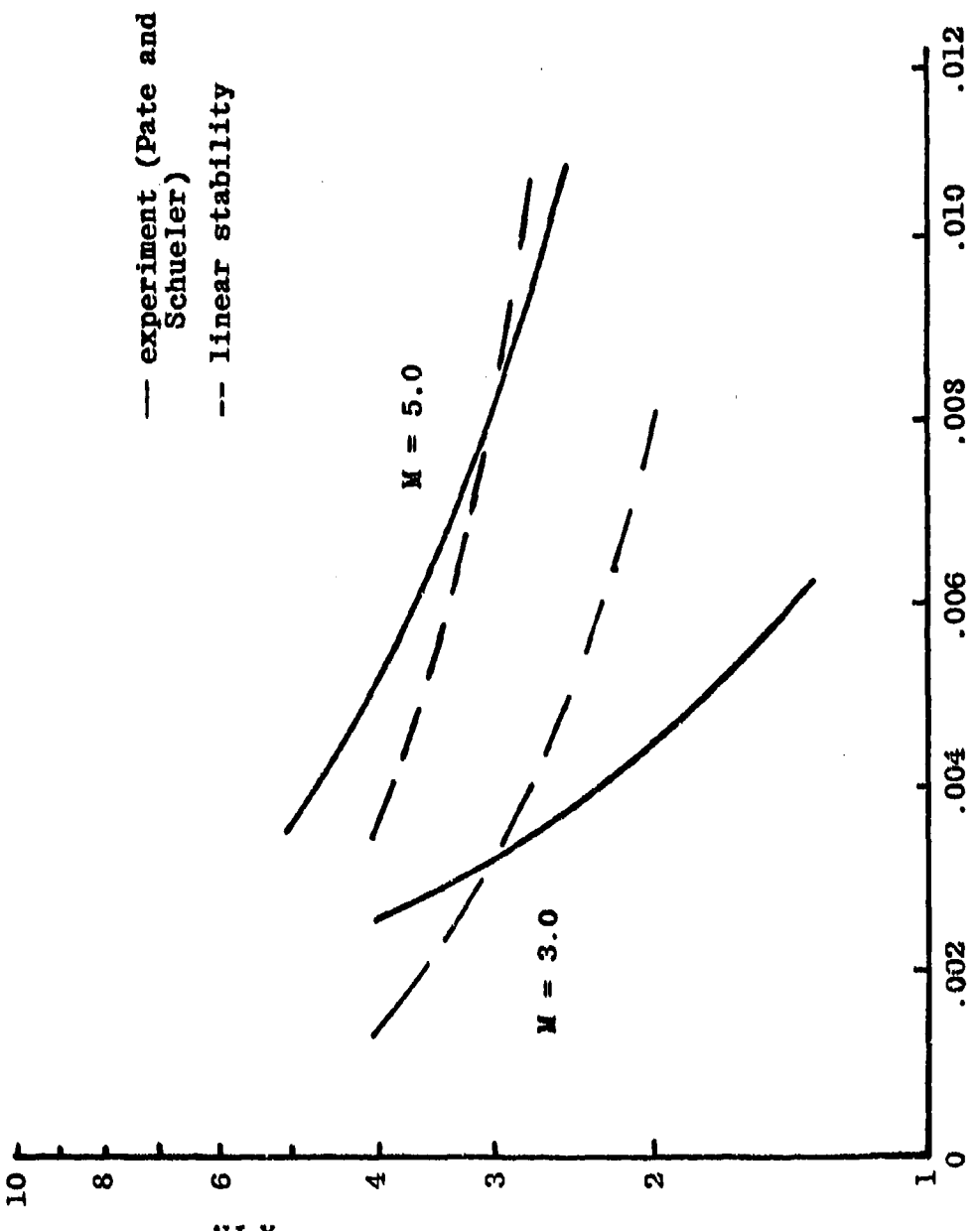

Fig. 2 Predicted effect of Reynolds Number-per-Inch on Transition in Wind Tunnel (end of transition).

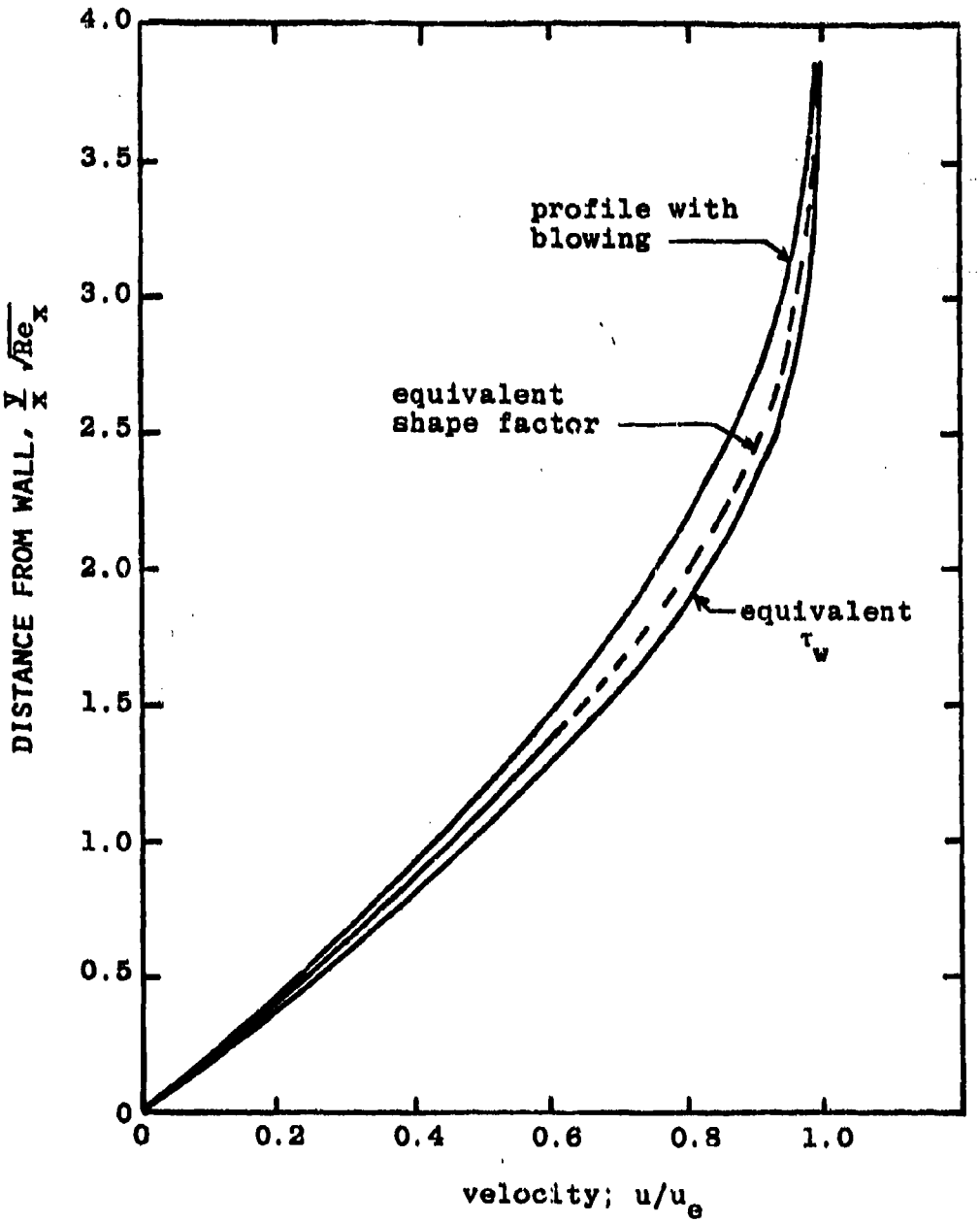

Fig. 3 Comparison of Blown Boundary-Layer Velocity Profile with Equivalent Non-Blown Profiles.

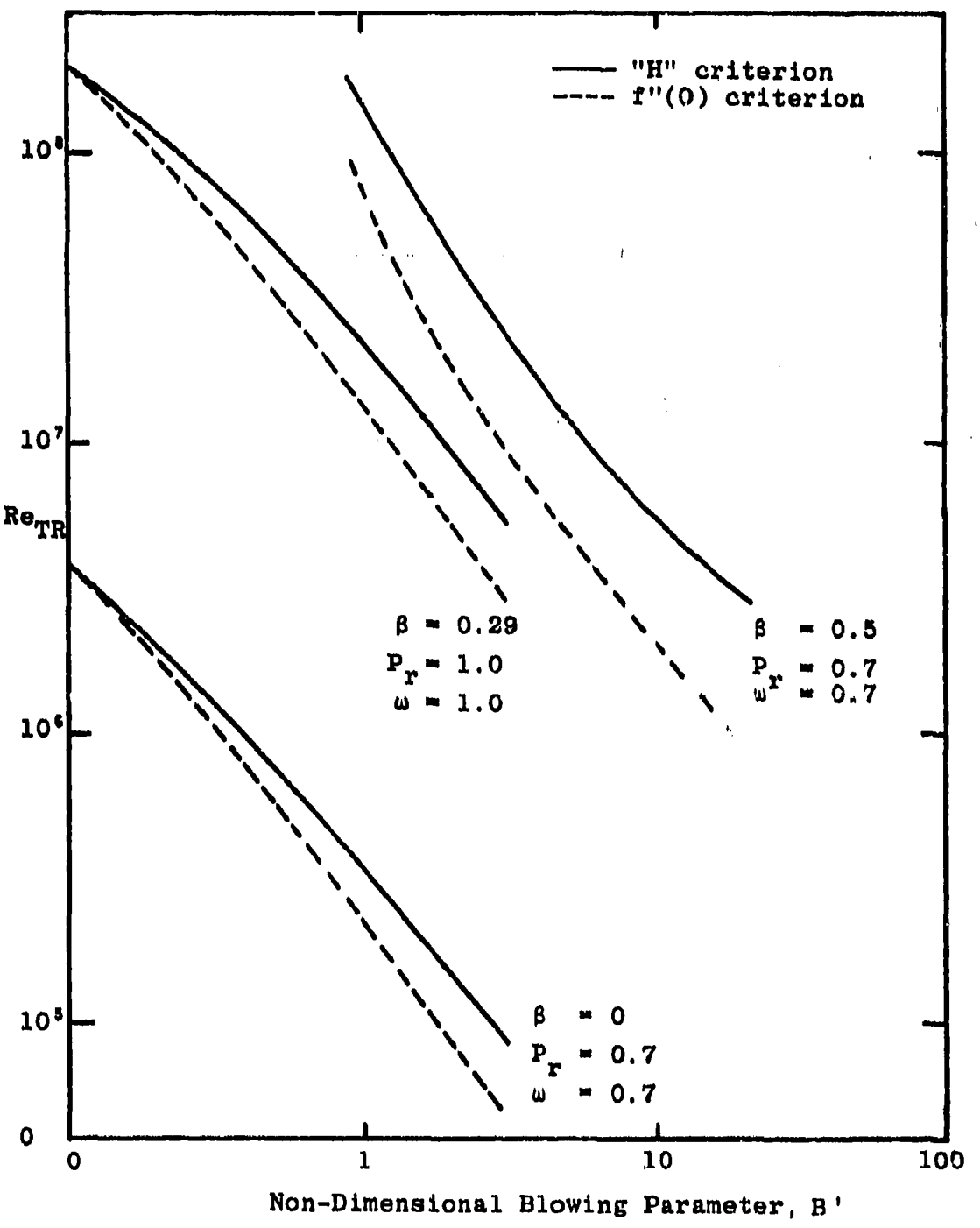

Fig. 4 Predicted Effect of Blowing on Transition Reynolds Number at $M_e = 0$.

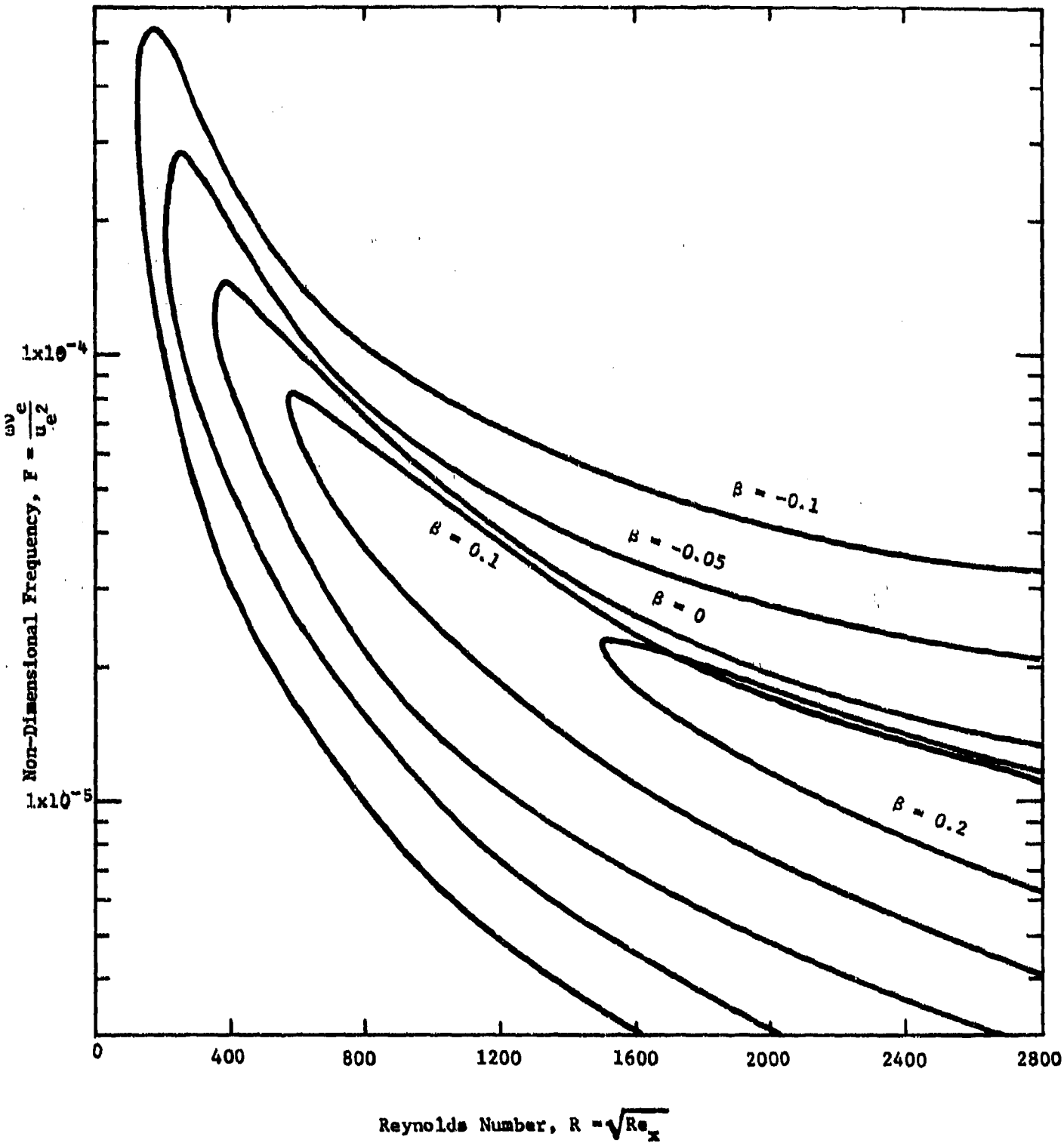

Fig. 5 Neutral Stability Curves for Several Values of the Falkner-Skan Pressure Gradient Parameter.

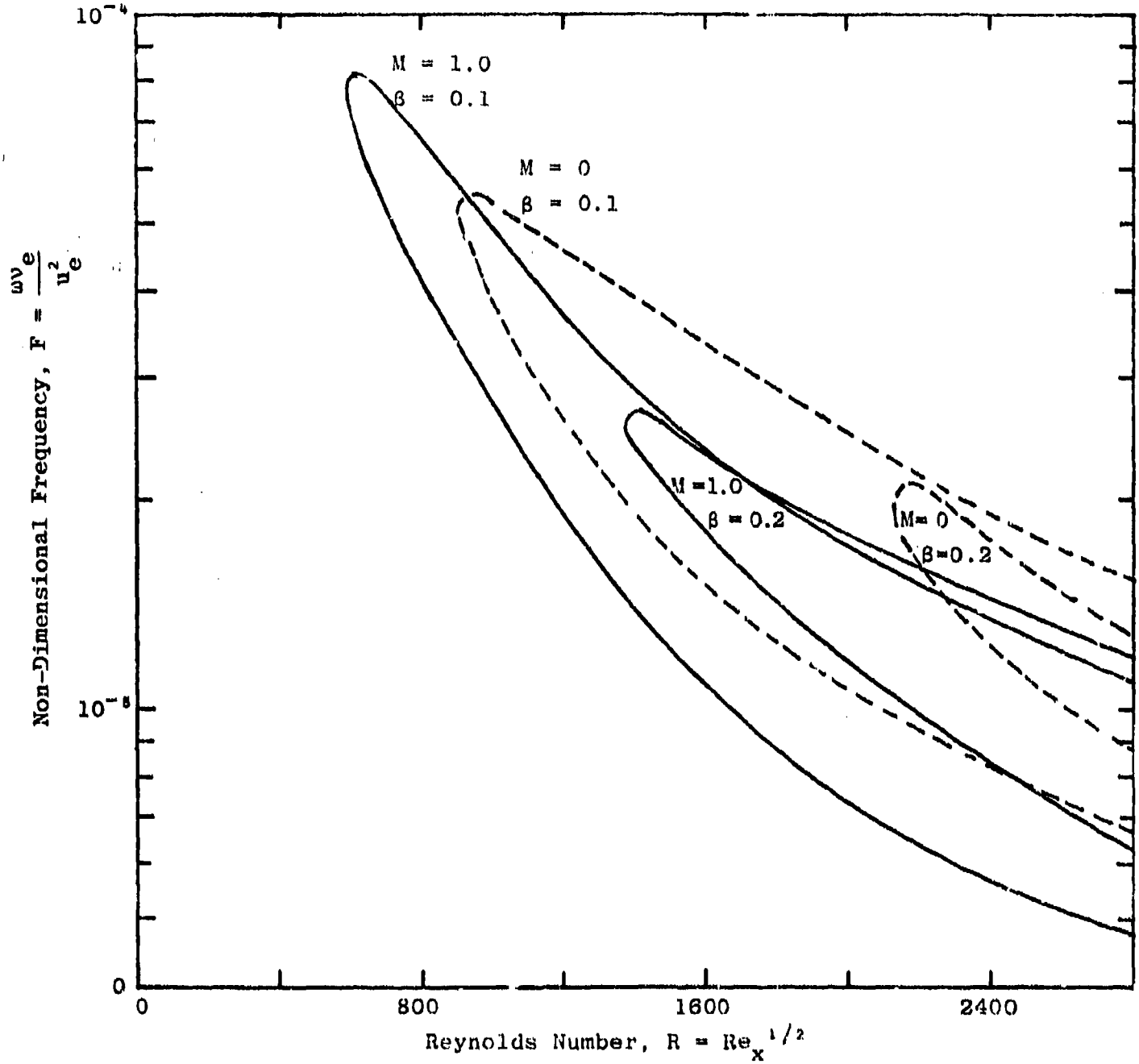

Fig. 6.a Comparison of Neutral Stability Curves at M = 0 and M = 1 Favorable Pressure Gradient.

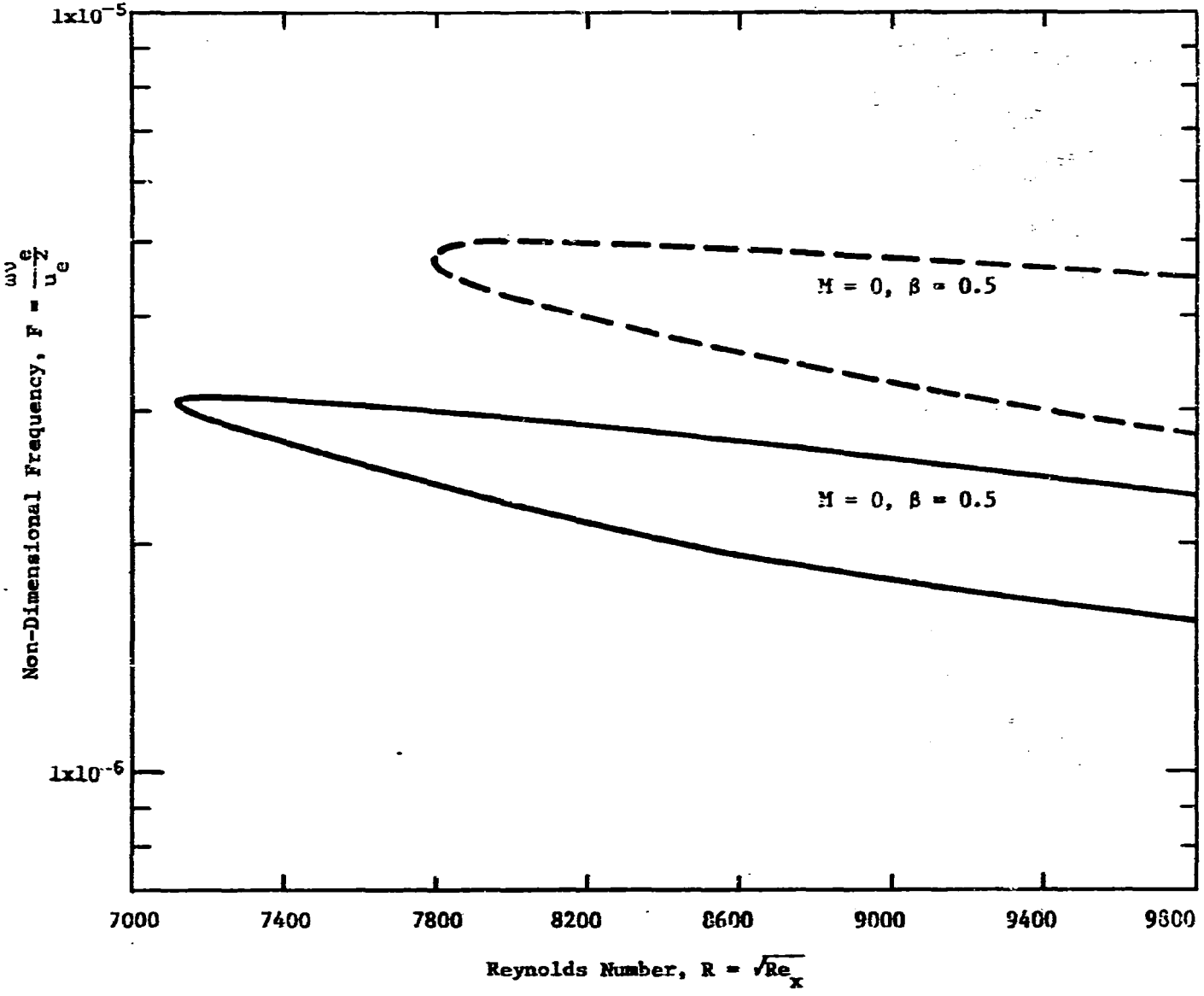

Fig. 6.b Neutral Stability Curves at M = 0 and M = 1
Favorable Pressure Gradient, β = 0.5

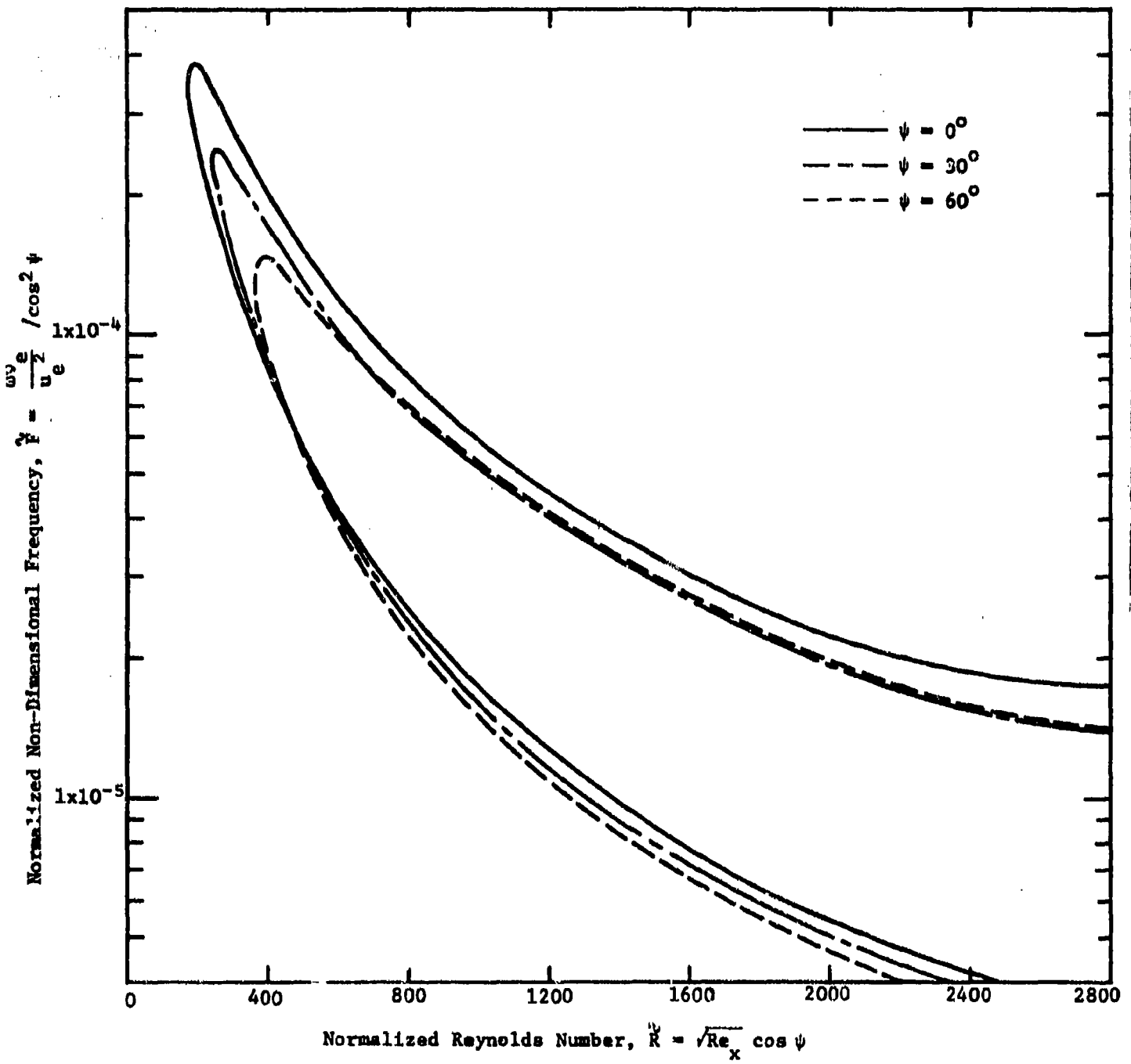

Fig. 7 Neutral Stability Curves for Waves Skewed at Angle ψ to Free-Stream Direction, Mach One.

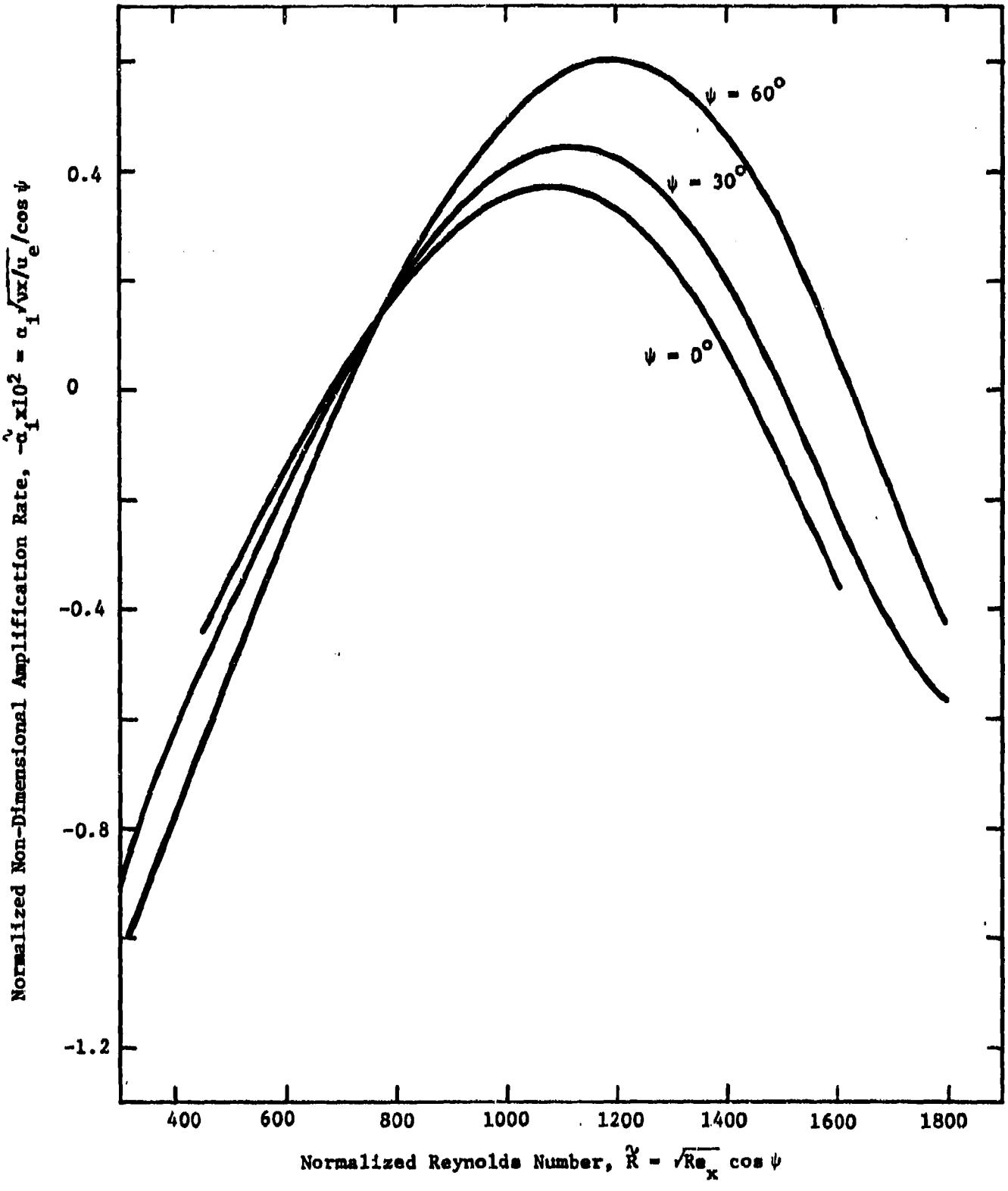

Fig. 8 Normalized Amplification Rate for Waves Skewed at angle ψ to Free-Stream. $\tilde{F} = 3x10^{-5}$, $\beta = 0$, Mach One.

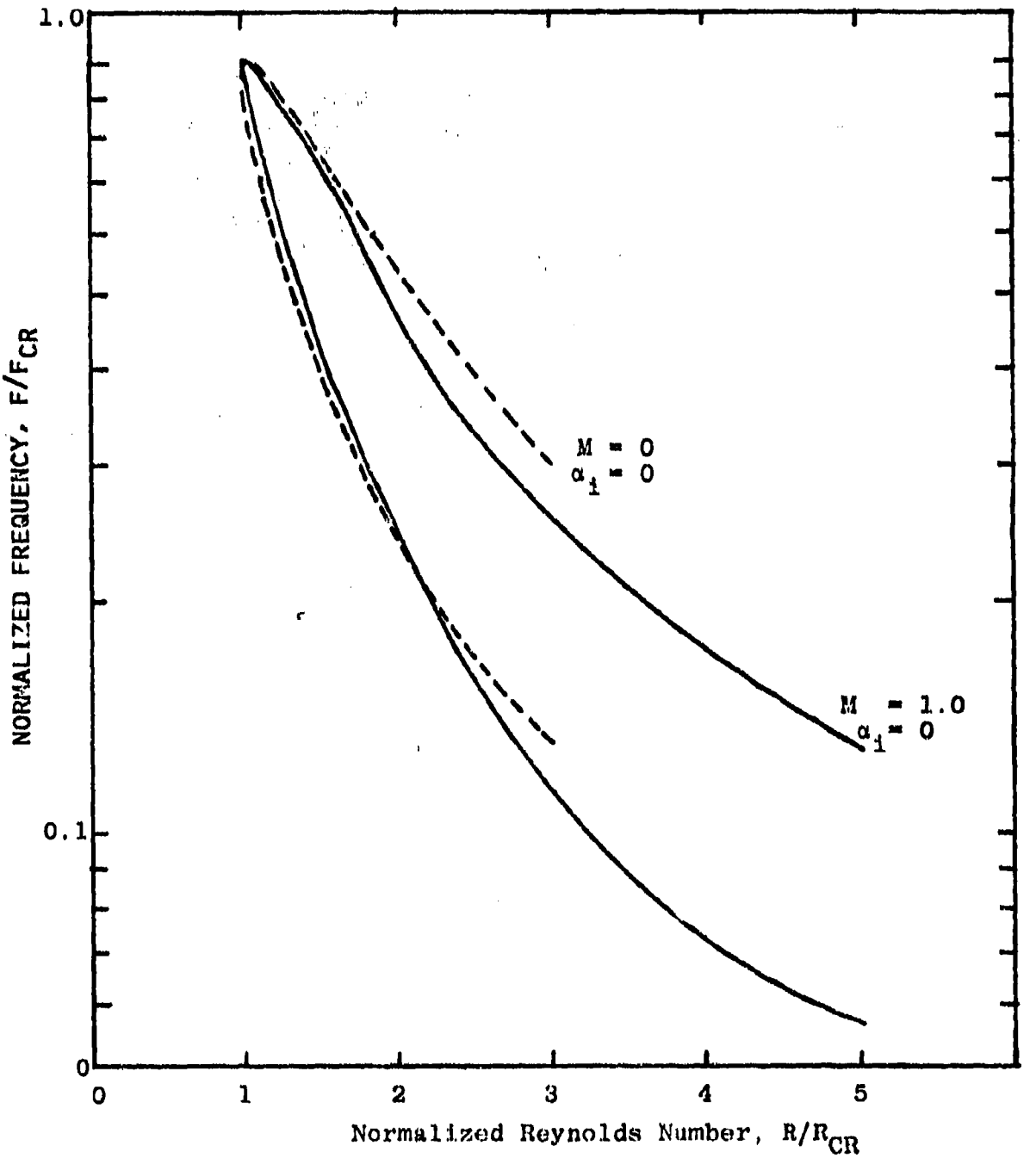

Fig. 9 NORMALIZED STABILITY MAPS FOR MACH NUMBERS ZERO AND ONE

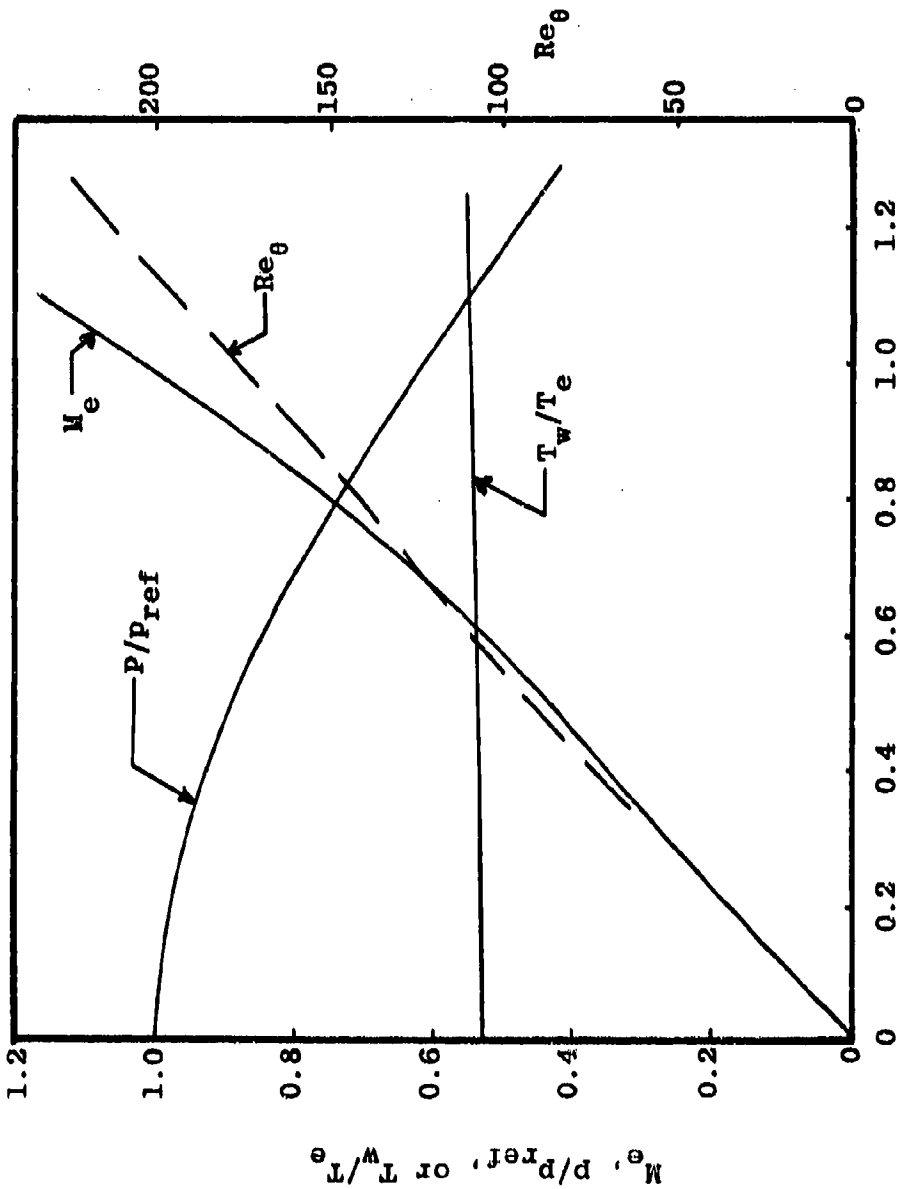

Fig. 19 Variations of Boundary-Layer Edge Conditions around a Nosetip.

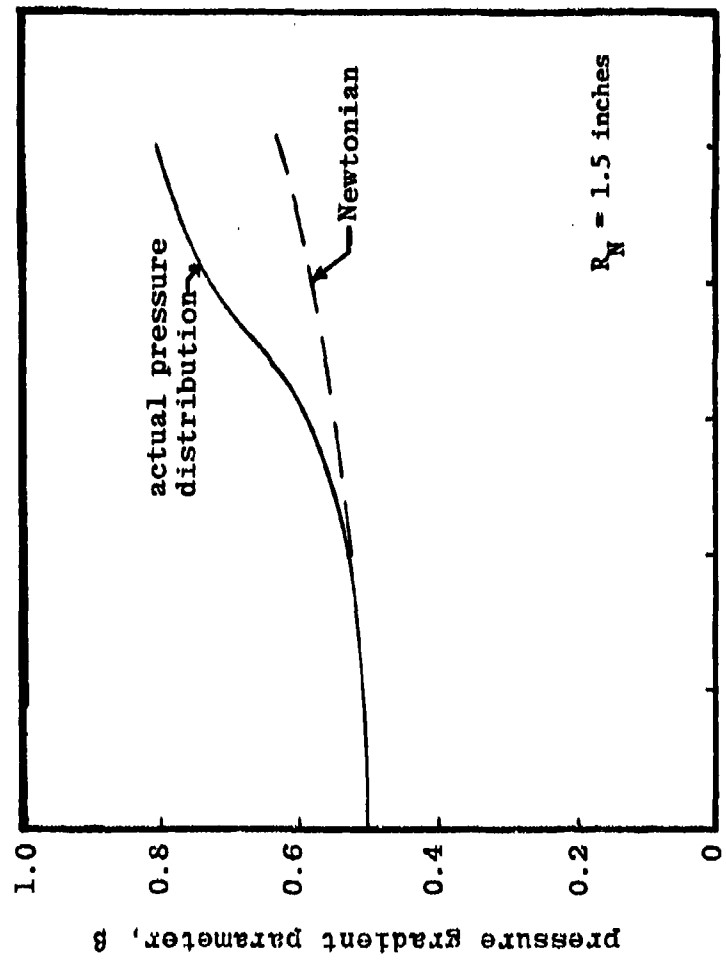

Fig. 11 Variation of Pressure Gradient Parameter around a Nosetip.

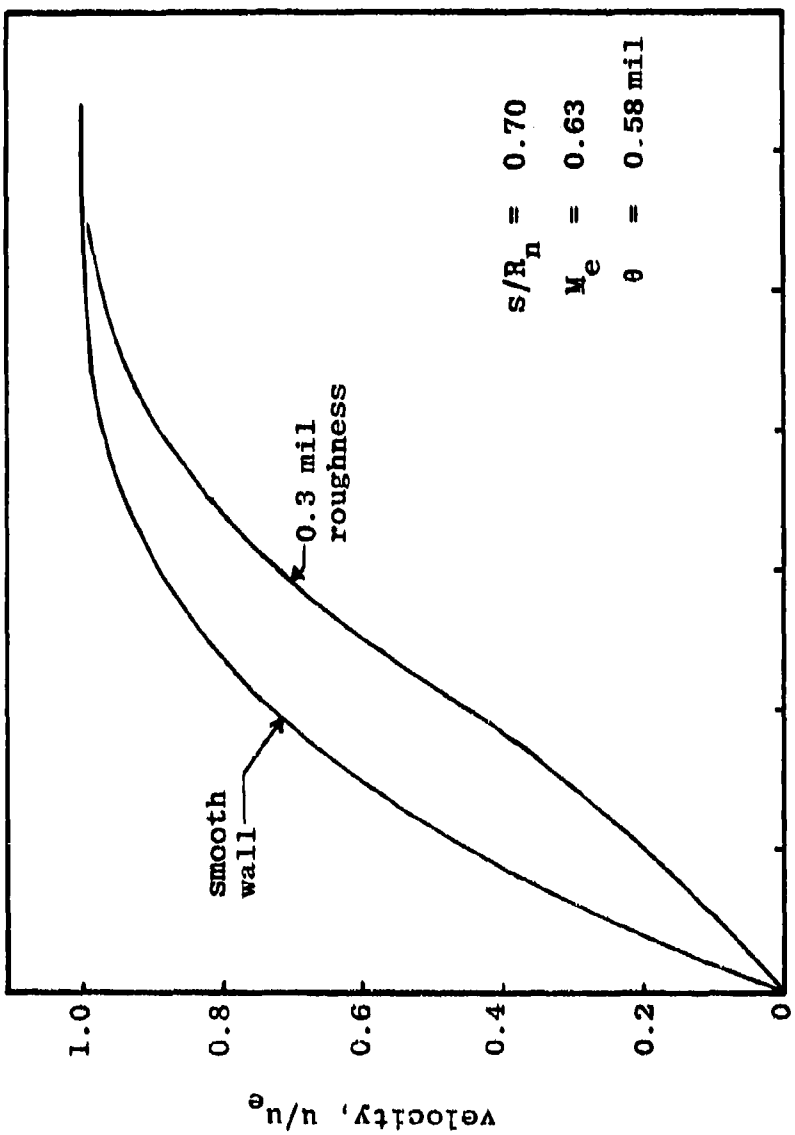

Fig. 12 Comparison of Mean-Velocity Profiles for Smooth and Rough-Walled Body.